

The flavor-dependent $U(1)_F$ model

Jin-Lei Yang^{1,2,3*}, Hai-Bin Zhang^{1,2,3†}, Tai-Fu Feng^{1,2,3‡}

Department of Physics, Hebei University, Baoding, 071002, China¹

*Key Laboratory of High-precision Computation and Application of
Quantum Field Theory of Hebei Province, Baoding, 071002, China²*

Research Center for Computational Physics of Hebei Province, Baoding, 071002, China³

Abstract

A flavor-dependent model (FDM) is proposed in this work. The model extends the Standard Model by an extra $U(1)_F$ local gauge group, two scalar doublets, one scalar singlet and two right-handed neutrinos, where the additional $U(1)_F$ charges are related to the particles' flavor. The new fermion sector in the FDM can explain the flavor mixings puzzle and the mass hierarchy puzzle simultaneously, and the nonzero Majorana neutrino masses can be obtained naturally by the Type I see-saw mechanism. In addition, the B meson rare decay processes $\bar{B} \rightarrow X_s \gamma$, $B_s^0 \rightarrow \mu^+ \mu^-$, the top quark rare decay processes $t \rightarrow ch$, $t \rightarrow uh$ and the τ lepton flavor violation processes $\tau \rightarrow 3e$, $\tau \rightarrow 3\mu$, $\mu \rightarrow 3e$ predicted in the FDM are analyzed.

* jlyang@hbu.edu.cn

† hbzhang@hbu.edu.cn

‡ fengtf@hbu.edu.cn

I. INTRODUCTION

The Standard Model (SM) achieves great success in describing the interactions of fundamental particles, and most of the observations coincide well with the SM predictions. However, the Yukawa couplings in the SM are still enigmatic, because the flavor mixings of quarks described by the Cabibbo-Kobayashi-Maskawa (CKM) matrix [1, 2] are not predicted from first principles in the SM, which is the so-called flavor puzzle. And the fermions of the three families have largely distinct masses

$$\frac{m_t}{m_c} \approx 104, \quad \frac{m_c}{m_u} \approx 773, \quad \frac{m_b}{m_s} \approx 51, \quad \frac{m_s}{m_d} \approx 20, \quad \frac{m_\tau}{m_\mu} \approx 17, \quad \frac{m_\mu}{m_e} \approx 207. \quad (1)$$

It exhibits the large hierarchical structure of masses across the three families while they share common SM gauge group quantum numbers, which is the so-called mass hierarchy puzzle. Meanwhile, the nonzero neutrino masses and mixings observed at the neutrino oscillation experiments [3] make the so-called flavor puzzle in the SM more acutely. All of these indicate that explaining the observed fermionic mass spectrum and mixings is one of the most enigmatic questions in particle physics, which may help understand the flavor nature and seek possible new physics (NP).

In literatures, there are some attempts to explain the fermionic mass hierarchies and flavor mixings. For example, the authors of Refs. [4–8] try to explain the fermionic flavor mixings by imposing the family symmetries, some proposals to explain the fermionic mass hierarchies can be found in Refs. [9–25]. The three-Higgs doublet model is motivated to account for the flavor structure with three generations of fermions [26–34], in which the number of Higgs doublets is three and has a flavor symmetry. A flavor-dependent $U(1)$ extension of the SM is proposed in Ref. [35], the authors explained the small mixing at quark sector by introducing a NP cut-off scale parameter. Weinberg proposed a new mechanism in which only the third generation of quarks and leptons achieve the masses at the tree level, while the masses for the second and first generations are produced by one-loop and two-loop radiative corrections respectively [20]. However, his analysis indicated that the ratios of the masses of the second and third generations fermions are independent of various masses of the third generation,

i.e.

$$\frac{m_c}{m_t} = \frac{m_s}{m_b} = \frac{m_\mu}{m_\tau} \quad \text{or} \quad \frac{m_c}{m_t^3} = \frac{m_s}{m_b^3} = \frac{m_\mu}{m_\tau^3},$$

which is not true of observed masses as shown in Eq. (1). Hence, he pointed out in his work that “this kind of NP models are not realistic for some reasons” [20]. In addition, Weinberg was the first to propose the Type I see-saw mechanism to give the tiny neutrino masses naturally [36], which provides one of the most popular mechanisms so far to give the tiny Majorana neutrino masses.

In this work, we adopt the Weinberg’s idea “only the third generation of fermions achieve the masses at the tree level”, but abandon “the masses for the second and first generations are produced by one-loop and two-loop radiative corrections respectively”. Instead, we propose to obtain the masses for the second and first generations by the “see-saw mechanism” (which is proposed by Weinberg to give the tiny Majorana neutrino masses as mentioned above), i.e. the masses for the second and first generations are produced by mixing with the third generation. In this case, the ratios of the masses of the second and third generations fermions depend on the tree-level mixing parameters of fermions, and we propose a flavor-dependent model (FDM) to realize this mechanism. The model extends the SM by an extra $U(1)_F$ local gauge group which relates to the particles’ flavor, two scalar doublets, one scalar singlet and two right-handed neutrinos. The new fermion sector in the FDM relates the fermionic flavor mixings to the fermionic mass hierarchies, which provides a new understanding about the mass hierarchy puzzle and the flavor mixing puzzle. In addition, the nonzero neutrino masses can be obtained naturally in the FDM by the Type I see-saw mechanism.

The paper is organized as follows: The structure of the FDM including particle content, scalar sector, fermion masses and gauge sector are collected in Sec. II. The numerical results of CKM matrix and Higgs masses predicted in the FDM are presented in Sec. III. The processes mediated by the flavor changed neutral currents (FCNCs) in the FDM are analyzed in Sec. IV. The summary is made in Sec. V.

Multiplets	$SU(3)_C$	$SU(2)_L$	$U(1)_Y$	$U(1)_F$
$l_1 = (\nu_{1L}, e_{1L})^T$	1	2	$-\frac{1}{2}$	z
$l_2 = (\nu_{2L}, e_{2L})^T$	1	2	$-\frac{1}{2}$	$-z$
$l_3 = (\nu_{3L}, e_{3L})^T$	1	2	$-\frac{1}{2}$	0
ν_{1R}	1	1	0	$-z$
ν_{2R}	1	1	0	z
e_{1R}	1	1	-1	$-z$
e_{2R}	1	1	-1	z
e_{3R}	1	1	-1	0
$q_1 = (u_{1L}, d_{1L})^T$	3	2	$\frac{1}{6}$	z
$q_2 = (u_{2L}, d_{2L})^T$	3	2	$\frac{1}{6}$	$-z$
$q_3 = (u_{3L}, d_{3L})^T$	3	2	$\frac{1}{6}$	0
d_{1R}	3	1	$-\frac{1}{3}$	$-z$
d_{2R}	3	1	$-\frac{1}{3}$	z
d_{3R}	3	1	$-\frac{1}{3}$	0
u_{1R}	3	1	$\frac{2}{3}$	$-z$
u_{2R}	3	1	$\frac{2}{3}$	z
u_{3R}	3	1	$\frac{2}{3}$	0
$\Phi_1 = (\phi_1^+, \phi_1^0)^T$	1	2	$\frac{1}{2}$	z
$\Phi_2 = (\phi_2^+, \phi_2^0)^T$	1	2	$\frac{1}{2}$	$-z$
$\Phi_3 = (\phi_3^+, \phi_3^0)^T$	1	2	$\frac{1}{2}$	0
χ	1	1	0	$2z$

TABLE I: Matter content in the FDM, where the nonzero constant z denotes the extra $U(1)_F$ charge.

II. THE FLAVOR-DEPENDENT MODEL

The gauge group of the FDM is $SU(3)_C \otimes SU(2)_L \otimes U(1)_Y \otimes U(1)_F$, where the extra $U(1)_F$ local gauge group is related to the particles' flavor. In the FDM, the third generation of

fermions obtain masses through the tree-level couplings with the SM scalar doublet, and the first two generations of fermions achieve masses through the tree-level mixings with the third generation as mentioned above. Hence, two additional scalar doublets are introduced in the FDM to realize the tree-level mixings of the first two generations and the third generation. In addition, to coincide with the observed neutrino oscillations, two right-handed neutrinos and one scalar singlet are introduced. Then the right-handed neutrinos obtain large Majorana masses after the scalar singlet achieving large vacuum expectation value (VEV), and the tiny neutrino masses and neutrino flavor mixings can be obtained by the Type I see-saw mechanism.

All fields in the FDM and the corresponding gauge symmetry charges are presented in Tab. I, where Φ_3 corresponds to the SM Higgs doublet, the nonzero constant z denotes the extra $U(1)_F$ charge. It can be noted in Tab. I that there are only two generations of right-handed neutrinos in the FDM, because both $U(1)_F$ and $U(1)_Y$ charges of the third generation of right-handed neutrinos ν_{R_3} are zero, which is trivial. In addition, it is obvious that the chiral anomaly cancellation can be guaranteed for the fermionic charges presented in Tab. I.

A. The scalar sector of the FDM

The scalar potential in the FDM can be written as

$$\begin{aligned}
V = & -M_{\Phi_1}^2 \Phi_1^\dagger \Phi_1 - M_{\Phi_2}^2 \Phi_2^\dagger \Phi_2 - M_{\Phi_3}^2 \Phi_3^\dagger \Phi_3 - M_\chi^2 \chi^* \chi + \lambda_\chi (\chi^* \chi)^2 + \lambda_1 (\Phi_1^\dagger \Phi_1)^2 \\
& + \lambda_2 (\Phi_2^\dagger \Phi_2)^2 + \lambda_3 (\Phi_3^\dagger \Phi_3)^2 + \lambda'_4 (\Phi_1^\dagger \Phi_1) (\Phi_2^\dagger \Phi_2) + \lambda''_4 (\Phi_1^\dagger \Phi_2) (\Phi_2^\dagger \Phi_1) \\
& + \lambda'_5 (\Phi_1^\dagger \Phi_1) (\Phi_3^\dagger \Phi_3) + \lambda''_5 (\Phi_1^\dagger \Phi_3) (\Phi_3^\dagger \Phi_1) + \lambda'_6 (\Phi_2^\dagger \Phi_2) (\Phi_3^\dagger \Phi_3) + \lambda''_6 (\Phi_2^\dagger \Phi_3) (\Phi_3^\dagger \Phi_2) \\
& + \lambda_7 (\Phi_1^\dagger \Phi_1) (\chi^* \chi) + \lambda_8 (\Phi_2^\dagger \Phi_2) (\chi^* \chi) + \lambda_9 (\Phi_3^\dagger \Phi_3) (\chi^* \chi) + [\lambda_{10} (\Phi_3^\dagger \Phi_1) (\Phi_3^\dagger \Phi_2) \\
& + \kappa (\Phi_1^\dagger \Phi_2) \chi + h.c.], \tag{2}
\end{aligned}$$

where

$$\Phi_1 = \begin{pmatrix} \phi_1^+ \\ \frac{1}{\sqrt{2}}(iA_1 + S_1 + v_1) \end{pmatrix}, \Phi_2 = \begin{pmatrix} \phi_2^+ \\ \frac{1}{\sqrt{2}}(iA_2 + S_2 + v_2) \end{pmatrix}, \Phi_3 = \begin{pmatrix} \phi_3^+ \\ \frac{1}{\sqrt{2}}(iA_3 + S_3 + v_3) \end{pmatrix},$$

$$\chi = \frac{1}{\sqrt{2}}(iA_\chi + S_\chi + v_\chi), \quad (3)$$

and v_i ($i = 1, 2, 3$), v_χ are the VEVs of Φ_i , χ respectively.

Based on the scalar potential in Eq. (2), the tadpole equations in the FDM can be written as¹

$$\begin{aligned} M_{\Phi_1}^2 &= \lambda_1 v_1^2 + \frac{1}{2} [(\lambda'_4 + \lambda''_4)v_2^2 + (\lambda'_5 + \lambda''_5)v_3^2 + \frac{v_2}{v_1}v_3^2 \text{Re}(\lambda_{10}) + \sqrt{2}\frac{v_2}{v_1}v_\chi \text{Re}(\kappa) + \lambda_7 v_\chi^2], \\ M_{\Phi_2}^2 &= \lambda_2 v_2^2 + \frac{1}{2} [(\lambda'_4 + \lambda''_4)v_1^2 + (\lambda'_6 + \lambda''_6)v_3^2 + \frac{v_1}{v_2}v_3^2 \text{Re}(\lambda_{10}) + \sqrt{2}\frac{v_1}{v_2}v_\chi \text{Re}(\kappa) + \lambda_8 v_\chi^2], \\ M_{\Phi_3}^2 &= \lambda_3 v_3^2 + \text{Re}(\lambda_{10})v_1 v_2 + \frac{1}{2} [(\lambda'_5 + \lambda''_5)v_1^2 + (\lambda'_6 + \lambda''_6)v_2^2 + \lambda_9 v_c^2], \\ M_\chi^2 &= \lambda_\chi v_\chi^2 + \frac{1}{2} [\lambda_7 v_1^2 + \lambda_8 v_2^2 + \lambda_9 v_3^2 + \sqrt{2}\frac{v_1 v_2}{v_\chi} \text{Re}(\kappa)]. \end{aligned} \quad (4)$$

On the basis (S_1, S_2, S_3, S_χ) , the CP-even Higgs squared mass matrix in the FDM is

$$M_h^2 = \begin{pmatrix} M_{h,11}^2 & M_{h,12}^2 & M_{h,13}^2 & M_{h,14}^2 \\ M_{h,12}^2 & M_{h,22}^2 & M_{h,23}^2 & M_{h,24}^2 \\ M_{h,13}^2 & M_{h,23}^2 & M_{h,33}^2 & M_{h,34}^2 \\ M_{h,14}^2 & M_{h,24}^2 & M_{h,34}^2 & M_{h,44}^2 \end{pmatrix}, \quad (5)$$

where

$$\begin{aligned} M_{h,11}^2 &= 2\lambda_1 v_1^2 - \frac{v_2}{2v_1} [v_3^2 \text{Re}(\lambda_{10}) + \sqrt{2}v_\chi \text{Re}(\kappa)], \\ M_{h,22}^2 &= 2\lambda_2 v_2^2 - \frac{v_1}{2v_2} [v_3^2 \text{Re}(\lambda_{10}) + \sqrt{2}v_\chi \text{Re}(\kappa)], \\ M_{h,33}^2 &= 2\lambda_3 v_3^2, \quad M_{h,44}^2 = 2\lambda_\chi v_\chi^2 - \frac{\sqrt{2}v_1 v_2}{2v_\chi} \text{Re}(\kappa), \\ M_{h,12}^2 &= (\lambda'_4 + \lambda''_4)v_1 v_2 + \frac{1}{2} \text{Re}(\lambda_{10})v_3^2 + \frac{\sqrt{2}}{2} \text{Re}(\kappa)v_\chi, \\ M_{h,13}^2 &= (\lambda'_5 + \lambda''_5)v_1 v_3 + \text{Re}(\lambda_{10})v_2 v_3, \quad M_{h,14}^2 = \lambda_7 v_1 v_\chi + \frac{\sqrt{2}}{2} \text{Re}(\kappa)v_2, \end{aligned}$$

¹ Calculating the exact vacuum stability conditions for any new physics model is difficult generally, and the obtained tadpole equations can be used to calculate the stationary points. In this case, we apply tadpole equations in the calculations, and guarantee the stability of vacuum numerically by keeping the scalar potential at the input v_1, v_2, v_3, v_χ are smaller than all the other stationary points.

$$\begin{aligned}
M_{h,23}^2 &= (\lambda'_6 + \lambda''_6)v_2v_3 + \text{Re}(\lambda_{10})v_1v_3, & M_{h,24}^2 &= \lambda_8v_2v_\chi + \frac{\sqrt{2}}{2}\text{Re}(\kappa)v_1, \\
M_{h,34}^2 &= \lambda_9v_3v_\chi.
\end{aligned} \tag{6}$$

The tadpole equations in Eq. (4) are used to obtain the matrix elements above.

Then, on the basis (A_1, A_2, A_3, A_χ) , the squared mass matrix of CP-odd Higgs in the FDM can be written as

$$M_A^2 = \begin{pmatrix} M_{A,11}^2 & M_{A,12}^2 & M_{A,13}^2 & M_{A,14}^2 \\ M_{A,12}^2 & M_{A,22}^2 & M_{A,23}^2 & M_{A,24}^2 \\ M_{A,13}^2 & M_{A,23}^2 & M_{A,33}^2 & M_{A,34}^2 \\ M_{A,14}^2 & M_{A,24}^2 & M_{A,34}^2 & M_{A,44}^2 \end{pmatrix}, \tag{7}$$

where

$$\begin{aligned}
M_{A,11}^2 &= -\frac{v_2}{2v_1}[\text{Re}(\lambda_{10})v_3^2 + \sqrt{2}v_\chi\text{Re}(\kappa)], & M_{A,33}^2 &= -2\text{Re}(\lambda_{10})v_1v_2, \\
M_{A,22}^2 &= -\frac{v_1}{2v_2}[\text{Re}(\lambda_{10})v_3^2 + \sqrt{2}v_\chi\text{Re}(\kappa)], & M_{A,44}^2 &= -\frac{\sqrt{2}v_1v_2}{2v_\chi}\text{Re}(\kappa), \\
M_{A,12}^2 &= \frac{\sqrt{2}}{2}v_\chi\text{Re}(\kappa) - \frac{1}{2}\text{Re}(\lambda_{10})v_3^2, & M_{A,13}^2 &= \text{Re}(\lambda_{10})v_2v_3, \\
M_{A,14}^2 &= \frac{\sqrt{2}}{2}v_2\text{Re}(\kappa), & M_{A,23}^2 &= \text{Re}(\lambda_{10})v_1v_3, & M_{A,24}^2 &= -\frac{\sqrt{2}}{2}v_1\text{Re}(\kappa), \\
M_{A,34}^2 &= 0.
\end{aligned} \tag{8}$$

On the basis $(\phi_1^+, \phi_2^+, \phi_3^+)$ and $(\phi_1^-, \phi_2^-, \phi_3^-)^T$, the squared mass matrix of singly charged Higgs in the FDM can be written as

$$M_{H^\pm}^2 = \begin{pmatrix} M_{H^\pm,11}^2 & M_{H^\pm,12}^2 & M_{H^\pm,13}^2 \\ (M_{H^\pm,12}^2)^* & M_{H^\pm,22}^2 & M_{H^\pm,23}^2 \\ (M_{H^\pm,13}^2)^* & (M_{H^\pm,23}^2)^* & M_{H^\pm,33}^2 \end{pmatrix}, \tag{9}$$

where

$$M_{H^\pm,11}^2 = -\frac{v_2}{2v_1}[\text{Re}(\lambda_{10})v_3^2 + \sqrt{2}v_\chi\text{Re}(\kappa)] - \frac{1}{2}(\lambda_4''v_2^2 + \lambda_5''v_3^2),$$

$$\begin{aligned}
M_{H^\pm,22}^2 &= -\frac{v_1}{2v_2}[\text{Re}(\lambda_{10})v_3^2 + \sqrt{2}v_\chi\text{Re}(\kappa)] - \frac{1}{2}(\lambda_4''v_1^2 + \lambda_6''v_3^2), \\
M_{H^\pm,33}^2 &= -\text{Re}(\lambda_{10})v_1v_2 - \frac{1}{2}(\lambda_5''v_1^2 + \lambda_6''v_2^2), \\
M_{H^\pm,12}^2 &= \frac{\sqrt{2}}{2}v_\chi\kappa + \frac{1}{2}\lambda_4''v_1v_2, \quad M_{H^\pm,13}^2 = \frac{1}{2}v_3(\lambda_5''v_1 + \lambda_{10}^*v_2), \\
M_{H^\pm,23}^2 &= \frac{1}{2}v_3(\lambda_6''v_2 + \lambda_{10}^*v_1). \tag{10}
\end{aligned}$$

It is easy to verify that there are two neutral Goldstones and one singly charged Goldstone in the FDM.

B. The fermion masses in the FDM

Based on the matter content listed in Tab. I, the Yukawa couplings in the FDM can be written as

$$\begin{aligned}
\mathcal{L}_Y &= Y_u^{33}\bar{q}_3\tilde{\Phi}_3u_{R3} + Y_d^{33}\bar{q}_3\Phi_3d_{R3} + Y_u^{32}\bar{q}_3\tilde{\Phi}_1u_{R2} + Y_u^{23}\bar{q}_2\tilde{\Phi}_1u_{R3} + Y_d^{32}\bar{q}_3\Phi_2d_{R2} \\
&+ Y_d^{23}\bar{q}_2\Phi_2d_{R3} + Y_u^{21}\bar{q}_2\tilde{\Phi}_3u_{R1} + Y_u^{12}\bar{q}_1\tilde{\Phi}_3u_{R2} + Y_d^{21}\bar{q}_2\Phi_3d_{R1} + Y_d^{12}\bar{q}_1\Phi_3d_{R2} \\
&+ Y_u^{31}\bar{q}_3\tilde{\Phi}_2u_{R1} + Y_u^{13}\bar{q}_1\tilde{\Phi}_2u_{R3} + Y_d^{31}\bar{q}_3\Phi_1d_{R1} + Y_d^{13}\bar{q}_1\Phi_1d_{R3} \\
&+ Y_e^{33}\bar{l}_3\Phi_3e_{R3} + Y_e^{32}\bar{l}_3\Phi_2e_{R2} + Y_e^{23}\bar{l}_2\Phi_2e_{R3} + Y_e^{21}\bar{l}_2\Phi_3e_{R1} + Y_e^{12}\bar{l}_1\Phi_3e_{R2} \\
&+ Y_e^{31}\bar{l}_3\Phi_1e_{R1} + Y_e^{13}\bar{l}_1\Phi_1e_{R3} + Y_R^{11}\bar{\nu}_{R1}^c\nu_{R1}\chi + Y_R^{22}\bar{\nu}_{R2}^c\nu_{R2}\chi^* + Y_D^{21}\bar{l}_2\tilde{\Phi}_3\nu_{R1} \\
&+ Y_D^{12}\bar{l}_1\tilde{\Phi}_3\nu_{R2} + Y_D^{31}\bar{l}_3\tilde{\Phi}_2\nu_{R1} + Y_D^{32}\bar{l}_3\tilde{\Phi}_1\nu_{R2} + h.c., \tag{11}
\end{aligned}$$

Then the mass matrices of quarks and leptons can be written as

$$m_q = \begin{pmatrix} 0 & m_{q,12} & m_{q,13} \\ m_{q,12}^* & 0 & m_{q,23} \\ m_{q,13}^* & m_{q,23}^* & m_{q,33} \end{pmatrix}, \quad m_e = \begin{pmatrix} 0 & m_{e,12} & m_{e,13} \\ m_{e,12}^* & 0 & m_{e,23} \\ m_{e,13}^* & m_{e,23}^* & m_{e,33} \end{pmatrix}, \quad m_\nu = \begin{pmatrix} 0 & M_D^T \\ M_D & M_R \end{pmatrix}, \tag{12}$$

where $q = u, d$, the parameters $m_{q,33}$ and $m_{e,33}$ are real, M_D is 2×3 Dirac mass matrix and M_R is 2×2 Majorana mass matrix (the nonzero neutrino masses are obtained by the Type I see-saw mechanism). The elements of the matrices in Eq. (12) are

$$m_{u,11} = m_{u,22} = 0, \quad m_{u,33} = \frac{1}{\sqrt{2}}Y_u^{33}v_3, \quad m_{u,12} = \frac{1}{\sqrt{2}}Y_u^{12}v_3, \quad m_{u,13} = \frac{1}{\sqrt{2}}Y_u^{13}v_1,$$

$$m_{u,23} = \frac{1}{\sqrt{2}}Y_u^{23}v_2, \quad (13)$$

$$m_{d,11} = m_{d,22} = 0, \quad m_{d,33} = \frac{1}{\sqrt{2}}Y_d^{33}v_3, \quad m_{d,12} = \frac{1}{\sqrt{2}}Y_d^{12}v_3, \quad m_{d,13} = \frac{1}{\sqrt{2}}Y_d^{13}v_1, \\ m_{d,23} = \frac{1}{\sqrt{2}}Y_d^{23}v_2, \quad (14)$$

$$m_{e,11} = m_{e,22} = 0, \quad m_{e,33} = \frac{1}{\sqrt{2}}Y_e^{33}v_3, \quad m_{e,12} = \frac{1}{\sqrt{2}}Y_e^{12}v_3, \quad m_{e,13} = \frac{1}{\sqrt{2}}Y_e^{13}v_1, \\ m_{e,23} = \frac{1}{\sqrt{2}}Y_e^{23}v_2, \quad (15)$$

$$M_{D,11} = M_{D,22} = 0, \quad M_{D,12} = \frac{1}{\sqrt{2}}Y_D^{12}v_3, \quad M_{D,31} = \frac{1}{\sqrt{2}}Y_D^{31}v_1, \\ M_{D,32} = \frac{1}{\sqrt{2}}Y_D^{32}v_2, \quad M_{R,12} = M_{R,21} = 0, \quad M_{R,11} = \frac{1}{\sqrt{2}}Y_R^{11}v_\chi, \quad M_{R,22} = \frac{1}{\sqrt{2}}Y_R^{22}v_\chi. \quad (16)$$

C. The gauge sector of the FDM

Due to the introducing of an extra $U(1)_F$ local gauge group in the FDM, the covariant derivative corresponding to $SU(2)_L \otimes U(1)_Y \otimes U(1)_F$ is defined as

$$D_\mu = \partial_\mu + ig_2 T_j A_{j\mu} + ig_1 Y B_\mu + ig_F F B'_\mu + ig_{Y_F} Y B'_\mu, \quad (j = 1, 2, 3), \quad (17)$$

where (g_2, g_1, g_F) , (T_j, Y, F) , $(A_{j\mu}, B_\mu, B'_\mu)$ denote the gauge coupling constants, generators and gauge bosons of groups $(SU(2)_L, U(1)_Y, U(1)_F)$ respectively, g_{Y_F} is the gauge coupling constant arises from the gauge kinetic mixing effect which presents in the models with two Abelian groups. Then the W boson mass can be written as

$$M_W = \frac{1}{2}g_2(v_1^2 + v_2^2 + v_3^2)^{1/2}, \quad (18)$$

where $(v_1^2 + v_2^2 + v_3^2)^{1/2} = v \approx 246$ GeV and we have $v_1, v_2 < v_3$ in the FDM. The γ , Z and Z' boson masses in the FDM can be written as

$$M_\gamma = 0, \quad M_Z \approx \frac{1}{2}(g_1^2 + g_2^2)^{1/2}v, \quad M_{Z'} \approx 2|zg_F|v_\chi, \quad (19)$$

and

$$\gamma = c_W B + s_W A_3, \quad Z = -s_W B + c_W A_3 + s'_W B', \quad Z' = s'_W (s_W B - c_W A_3) + c'_W B', \quad (20)$$

where γ , Z , Z' are the mass eigenstates, $c_W \equiv \cos \theta_W$, $s_W \equiv \sin \theta_W$ with θ_W denoting the Weinberg angle, $s'_W \equiv \sin \theta'_W$, $c'_W \equiv \cos \theta'_W$ with θ'_W representing the $Z - Z'$ mixing effect.

III. CKM MATRIX AND HIGGS MASSES IN THE FDM

The quark sector in the FDM are redefined and the additional two scalar doublets, one scalar singlet modify the scalar potential of the model, hence we focus on the quark sector and scalar sector of the model in this section.

A. CKM matrix

The analysis in our previous work [37] shows that the quark mass matrices obtained in the FDM can fit the measured CKM matrix well. In this work, we perform a χ^2 test to explore the best fit describing the quark masses and CKM matrix in the model. Generally, the χ^2 function can be constructed as

$$\chi^2 = \sum_1 \left(\frac{O_i^{\text{th}} - O_i^{\text{exp}}}{\sigma_i^{\text{exp}}} \right)^2, \quad (21)$$

where O_i^{th} denotes the i -th observable computed theoretically, O_i^{exp} is the corresponding experimental value and σ_i^{exp} is the uncertainty in O_i^{exp} . Taking into account 10 observables including 6 quark masses, 3 mixing angles and a phase in the CKM matrix, we scan the parameter space

$$|m_{u,13}| = (0.0 \sim 1.0) \text{ GeV}, |m_{d,13}| = (0.0 \sim 0.1) \text{ GeV}, \theta_{q,ij} = (-\pi, \pi) \quad (22)$$

with $m_{q,ij} = |m_{q,ij}|e^{i\theta_{q,ij}}$, $q = u, d$, $ij = 12, 13, 23$. Then we obtain the best fit solution corresponding to $\chi^2 = 0.0072$, the results of this fit are listed in Tab. II where various O_i^{exp} we use are listed in the third column and σ_i^{exp} are take from PDG [3]. The parameters for the best fit listed in Tab. II are

$$\begin{aligned} |m_{u,13}| &= 0.3152 \text{ GeV}, \theta_{u,12} = -0.8248\pi, \theta_{u,13} = 0.1231\pi, \theta_{u,23} = -0.1129\pi, \\ |m_{d,13}| &= 7.235 \text{ MeV}, \theta_{d,12} = 0.6705\pi, \theta_{d,13} = -0.3622\pi, \theta_{d,23} = -0.06389\pi, \end{aligned} \quad (23)$$

Observables	O_i^{th}	O_i^{exp}	Deviations in %
$m_u[\text{MeV}]$	2.15	2.16	0.47
$m_c[\text{GeV}]$	1.67	1.67	0
$m_t[\text{GeV}]$	172.5	172.5	0
$m_d[\text{MeV}]$	4.67	4.67	0
$m_s[\text{MeV}]$	93.4	93.4	0
$m_b[\text{GeV}]$	4.78	4.78	0
$ v_{us} $	0.2253	0.2253	0
$ v_{ub} $	0.3616	0.003616	0
$ v_{cb} $	0.4149	0.04149	0

TABLE II: The results obtained for the best fit corresponding to $\chi^2 = \mathbf{0.0072}$.

and $|m_{q,12}|$, $|m_{q,23}|$, $m_{q,33}$ ($q = u, d$) can be obtained by²

$$\begin{aligned}
m_{q,33} &= m_{q_3} - m_{q_1} - m_{q_2}, \\
|m_{q,23}| &= [(m_{q_1} + m_{q_2})m_{q,33} - |m_{q,13}|^2]^{1/2}, \\
|m_{q,12}| &= \frac{|m_{q,13}||m_{q,23}|}{|m_{q,33}|} \cos(\theta_{q,12} + \theta_{q,23} - \theta_{q,13}) \\
&\quad + \left\{ \left[\frac{|m_{q,13}||m_{q,23}|}{|m_{q,33}|^2} \cos(\theta_{q,12} + \theta_{q,23} - \theta_{q,13}) \right]^2 + \frac{m_{q_1}m_{q_2}}{|m_{q,33}|^2} \right\}^{1/2} |m_{q,33}|, \quad (24)
\end{aligned}$$

with m_{q_k} being the k -generation quark q mass.

It is obvious that there are additional CP phases in the obtained CKM matrix by taking the parameters in Eq. (23) as inputs, but we do not list the observed CP phase in the CKM matrix in Tab. II. Because the CKM matrix is defined as

$$V_{\text{CKM}} = (U_L^u U_L^{d\dagger})^*, \quad (25)$$

where U_L^u , U_L^d are the unitary matrices which diagonalize the quark matrices in Eq. (12)

$$m_u^{\text{diag}} = U_L^{u*} m_u U_R^{u\dagger}, \quad m_d^{\text{diag}} = U_L^{d*} m_d U_R^{d\dagger}. \quad (26)$$

² Eq. (24) is obtained with the approximation $|m_{q,12}|$, $|m_{q,13}|$, $|m_{q,23}| \ll m_{q,33}$, and the terms of $\mathcal{O}(m_{q,ij}/m_{q,33})^3$ are neglected. For down type quark, higher order corrections to Eq. (24) are also important, we calculated them numerically and the corrections to $m_{q,33}$, $|m_{q,23}|$, $|m_{q,12}|$ are 9.32 MeV, -27.03 MeV, 0.196 MeV respectively.

Eq. (26) is invariant under

$$\begin{aligned} U_L^u &\rightarrow \text{diag}(e^{-i\theta_u}, e^{-i\theta_c}, e^{-i\theta_t}) \cdot U_L^u, & U_R^u &\rightarrow \text{diag}(e^{i\theta_u}, e^{i\theta_c}, e^{i\theta_t}) \cdot U_R^u, \\ U_L^d &\rightarrow \text{diag}(e^{i\theta_d}, e^{i\theta_s}, e^{i\theta_b}) \cdot U_L^d, & U_R^d &\rightarrow \text{diag}(e^{-i\theta_d}, e^{-i\theta_s}, e^{-i\theta_b}) \cdot U_R^d, \end{aligned} \quad (27)$$

so there are six free parameters $\theta_u, \theta_c, \theta_t, \theta_d, \theta_s, \theta_b$ which can absorb the extra CP phases in the obtained CKM matrix, these parameters are not observable. As a result, the observed CP phase in the CKM matrix can be obtained by defining appropriate $\theta_u, \theta_c, \theta_t, \theta_d, \theta_s, \theta_b$. This fact is always valid because there are also six possible CP violation parameters at the quark sector in the model.

B. Perturbative unitary bounds

The scalar sector of the FDM is extended by two scalar doublets and one scalar singlet, additional new couplings are also introduced correspondingly. Therefore, the tree-level perturbative unitary should be applied to the scalar elastic scattering processes in this model [38]. The zero partial wave amplitude

$$a_0 = \frac{1}{32\pi} \sqrt{\frac{4p_f^{\text{CM}} p_i^{\text{CM}}}{s}} \int_{-1}^{+1} T_{2 \rightarrow 2} d \cos \theta \quad (28)$$

must satisfy the condition $|\text{Re}(a_0)| \leq \frac{1}{2}$, where s is the centre of mass (CM) energy, $T_{2 \rightarrow 2}$ denotes the matrix element for $2 \rightarrow 2$ processes, θ is the incident angle between two incoming particles, p_i^{CM} and p_f^{CM} are the initial and final momenta in the CM system respectively.

The possible two particle states of $2 \rightarrow 2$ scattering processes at the scalar sector in the FDM are $S_1 S_1, S_2 S_2, S_3 S_3, S_\chi S_\chi, S_1 S_2, S_1 S_3, S_1 S_\chi, S_2 S_3, S_2 S_\chi, S_3 S_\chi$. Considering the limit $s \gg M_{S_1}^2, M_{S_2}^2, M_{S_3}^2, M_{S_\chi}^2$, we have

$$\begin{aligned} a_0^{S_1 S_1 \rightarrow S_1 S_1} &\approx \frac{1}{16\pi} (6\lambda_1), & a_0^{S_2 S_2 \rightarrow S_2 S_2} &\approx \frac{1}{16\pi} (6\lambda_2), \\ a_0^{S_3 S_3 \rightarrow S_3 S_3} &\approx \frac{1}{16\pi} (6\lambda_3), & a_0^{S_\chi S_\chi \rightarrow S_\chi S_\chi} &\approx \frac{1}{16\pi} (6\lambda_\chi), \\ a_0^{S_1 S_1 \rightarrow S_2 S_2} &\approx \frac{1}{16\pi} (\lambda'_4 + \lambda''_4), & a_0^{S_1 S_2 \rightarrow S_1 S_2} &\approx \frac{1}{16\pi} (\lambda'_4 + \lambda''_4), \\ a_0^{S_1 S_1 \rightarrow S_3 S_3} &\approx \frac{1}{16\pi} (\lambda'_5 + \lambda''_5), & a_0^{S_1 S_3 \rightarrow S_1 S_3} &\approx \frac{1}{16\pi} (\lambda'_5 + \lambda''_5), \end{aligned}$$

$$\begin{aligned}
a_0^{S_2S_2 \rightarrow S_3S_3} &\approx \frac{1}{16\pi}(\lambda'_6 + \lambda''_6), & a_0^{S_2S_3 \rightarrow S_2S_3} &\approx \frac{1}{16\pi}(\lambda'_6 + \lambda''_6), \\
a_0^{S_1S_1 \rightarrow S_\chi S_\chi} &\approx \frac{1}{16\pi}(\lambda_7), & a_0^{S_1S_\chi \rightarrow S_1S_\chi} &\approx \frac{1}{16\pi}(\lambda_7), \\
a_0^{S_2S_2 \rightarrow S_\chi S_\chi} &\approx \frac{1}{16\pi}(\lambda_8), & a_0^{S_2S_\chi \rightarrow S_2S_\chi} &\approx \frac{1}{16\pi}(\lambda_8), \\
a_0^{S_3S_3 \rightarrow S_\chi S_\chi} &\approx \frac{1}{16\pi}(\lambda_9), & a_0^{S_3S_\chi \rightarrow S_3S_\chi} &\approx \frac{1}{16\pi}(\lambda_9), \\
a_0^{S_3S_3 \rightarrow S_1S_2} &\approx \frac{1}{16\pi}[2\text{Re}(\lambda_{10})], & a_0^{S_1S_3 \rightarrow S_2S_3} &\approx \frac{1}{16\pi}[2\text{Re}(\lambda_{10})].
\end{aligned} \tag{29}$$

Requiring $|\text{Re}(a_0)| \leq \frac{1}{2}$ for each individual process, we have

$$\begin{aligned}
|\lambda_1|, |\lambda_2|, |\lambda_3|, |\lambda_\chi| &\leq \frac{4\pi}{3}, & |\text{Re}(\lambda_{10})| &\leq 4\pi, \\
|\lambda'_4 + \lambda''_4|, |\lambda'_5 + \lambda''_5|, |\lambda'_6 + \lambda''_6|, |\lambda_7|, |\lambda_8|, |\lambda_9| &\leq 8\pi.
\end{aligned} \tag{30}$$

C. Higgs masses in the FDM

For the free parameters in the scalar sector of the FDM, we take $v_1 = v_2$, $\lambda'_4 = \lambda''_4 = \lambda_4/2$, $\lambda'_5 = \lambda''_5 = \lambda_5/2$, $\lambda'_6 = \lambda''_6 = \lambda_6/2$ and all parameters to be real for simplicity. In addition, v_χ is limited by the new Z' boson mass as shown in Eq. (19), hence we take $v_\chi \geq 5$ TeV in the following analysis. Considering the perturbative unitary bounds presented in Eq. (30), we scan the following parameter space

$$\begin{aligned}
v_1 &= (0, 40) \text{ GeV}, & \lambda_i &= (0, 4) \text{ with } (i = 1, \dots, 9, \chi), & \lambda_{10} &= (-4, 0), \\
v_\chi &= (5, 40) \text{ TeV}, & \kappa &= (-3, -0.1) \text{ TeV},
\end{aligned} \tag{31}$$

to explore the Higgs mass spectrum in the FDM. In the scanning, we keep the next-to-lightest CP-even Higgs mass M_{H_2} in the range $124 \text{ GeV} < M_{H_2} < 126 \text{ GeV}$ and the scalar potential at the input v_1, v_2, v_3, v_χ are smaller than all the other stationary points to guarantee the stability of vacuum.

1. CP-even Higgs masses

The results of CP-even Higgs masses M_{H_1} versus v_1 , M_{H_3} versus κ , M_{H_4} versus v_χ are plotted in Fig. 1 (a), Fig. 1 (b), Fig. 1 (c) respectively. We do not present the results of

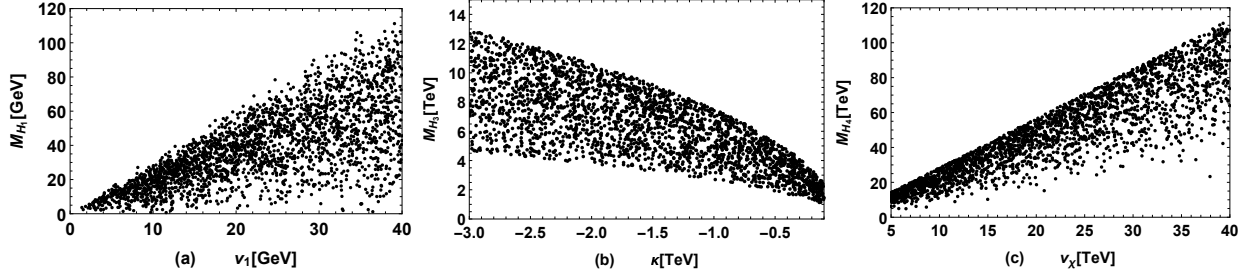


FIG. 1: The results of CP-even Higgs masses M_{H_1} (a), M_{H_3} (b), M_{H_4} (c) versus v_1 , κ , v_χ are plotted respectively by scanning the parameter space in Eq. (31).

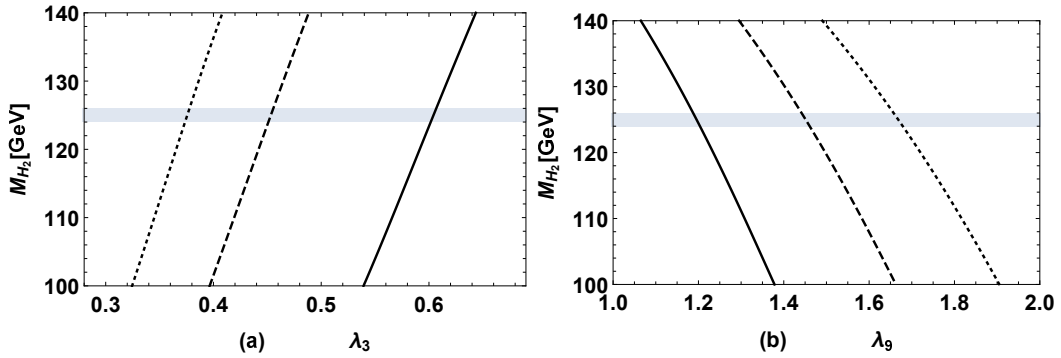


FIG. 2: The results of M_{H_2} versus λ_3 (a), λ_9 (b), where the solid, dashed, dotted curves denotes the results for $\lambda_\chi = 2, 3, 4$ respectively, and the gray areas denote the range $124 \text{ GeV} < M_{H_2} < 126 \text{ GeV}$.

the next-to-lightest CP-even Higgs mass M_{H_2} in Fig. 1 because M_{H_2} is limited in the range $124 \text{ GeV} < M_{H_2} < 126 \text{ GeV}$ in the plotting. Fig. 1 (a) shows that the lightest Higgs mass M_{H_1} in the FDM mainly depends on the chosen value of v_1 , and M_{H_1} can reach 95 GeV for $v_1 \gtrsim 30 \text{ GeV}$ which will be explored in detail in our next work. As shown in Fig. 1 (b) and (c), M_{H_3} , M_{H_4} are dominated by κ , v_χ , where M_{H_4} is about 110 TeV for large v_χ while M_{H_3} is about 13 TeV for large $|\kappa|$.

As mentioned above, Φ_3 corresponds to the SM Higgs doublet, hence λ_3 may affect the 125 GeV Higgs boson mass M_{H_2} significantly. In addition, Eq. (6) shows that there are large mixing effects between S_3 and S_χ , it indicates λ_9 , λ_χ can also affect M_{H_2} . And to verify numerically that M_{H_2} is mainly affected by λ_3 , λ_9 , λ_χ , we take $v_1 = 20 \text{ GeV}$, $\lambda_1 = \lambda_2 = \lambda_4 = \lambda_5 = \lambda_6 = \lambda_7 = \lambda_8 = 2$, $\lambda_{10} = -2$, $v_\chi = 10 \text{ TeV}$, $\kappa = -1 \text{ TeV}$ to explore the

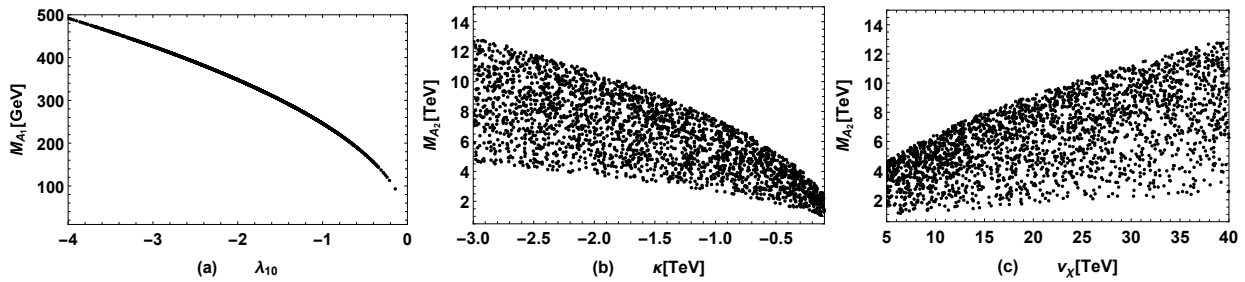


FIG. 3: The results of CP-even Higgs masses M_{A_1} (a), M_{A_2} (b), M_{A_2} (c) versus λ_{10} , κ , v_χ are plotted respectively by scanning the parameter space in Eq. (31).

effects of λ_3 , λ_9 , λ_χ on M_{H_2} . Then M_{H_2} versus λ_3 , λ_9 are plotted in Fig. 2 (a) and Fig. 2 (b) respectively, where the solid, dashed, dotted curves denotes the results for $\lambda_\chi = 2, 3, 4$ respectively, and the gray areas denote the range $124 \text{ GeV} < M_{H_2} < 126 \text{ GeV}$. The picture shows M_{H_2} increases with increasing λ_3 , λ_χ and decreases with increasing λ_9 , and λ_3 , λ_9 , λ_χ affect the theoretical predictions on M_{H_2} significantly.

2. CP-odd Higgs masses

There are two physical CP-odd Higgs in the FDM, and the results of CP-odd Higgs masses M_{A_1} versus λ_{10} , M_{A_2} versus κ , M_{A_2} versus v_χ are plotted in Fig. 3 (a), Fig. 3 (b), Fig. 3 (c) respectively. It is obvious in Fig. 3 (a) that M_{A_1} is dominated by the value of λ_{10} completely, and M_{A_1} increases with increasing $|\lambda_{10}|$. In addition, M_{A_2} is dominated by κ , v_χ as shown in Fig. 3 (b) and Fig. 3 (c), where M_{A_2} can be large when $|\kappa|$ and v_χ are large.

3. Charged Higgs masses

Similar to the case of CP-odd Higgs, there are also two physical charged Higgs in the FDM. The results of charged Higgs masses $M_{H_1^\pm}$ versus λ_{10} , $M_{H_2^\pm}$ versus κ , $M_{H_2^\pm}$ versus v_χ are plotted in Fig. 4 (a), Fig. 4 (b), Fig. 4 (c) respectively. Fig. 4 (a) indicates that $M_{H_1^\pm}$ is mainly affected by λ_{10} , but the other scanning parameter can also influence the predicted $M_{H_1^\pm}$ especially for small $|\lambda_{10}|$. Similar to the case of M_{A_2} , Fig. 4 (b) and Fig. 4 (c) show that $M_{H_2^\pm}$ is also dominated by κ , v_χ .

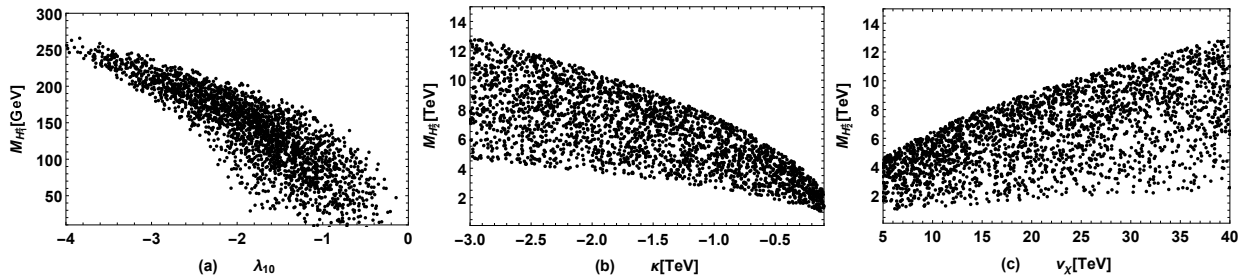


FIG. 4: The results of charged Higgs masses $M_{H_1^\pm}$ (a), $M_{H_2^\pm}$ (b), $M_{H_2^\pm}$ (c) versus λ_{10} , κ , v_χ are plotted respectively by scanning the parameter space in Eq. (31).

IV. THE FLAVOR CHANGED NEUTRAL CURRENTS IN THE FDM

As shown in Eq. (11), the different generations of fermions couple to different Higgs bosons while Φ_3 corresponding to the SM-like Higgs, which are quite different from the ones in the SM. In addition, the new defined Z and Z' gauge bosons can also mediate the FCNCs. Hence, observing the FCNCs in the FDM may be effective to test the model. In this section, we focus on the B meson rare decay processes $\bar{B} \rightarrow X_s \gamma$, $B_s^0 \rightarrow \mu^+ \mu^-$, the top quark rare decay processes $t \rightarrow ch$, $t \rightarrow uh$ and the charged lepton flavor violation processes $\tau \rightarrow 3e$, $\tau \rightarrow 3\mu$, $\mu \rightarrow 3e$ predicted in the FDM. And for simplicity, we take the nonzero $U_F(1)$ charge $z = 1$ in the following analysis.

A. B meson rare decay processes $\bar{B} \rightarrow X_s \gamma$ and $B_s^0 \rightarrow \mu^+ \mu^-$ in the FDM

The B meson rare decay processes $\bar{B} \rightarrow X_s \gamma$, $B_s^0 \rightarrow \mu^+ \mu^-$ are related closely to the NP contributions, and the average experimental data on the branching ratios of $\bar{B} \rightarrow X_s \gamma$, $B_s^0 \rightarrow \mu^+ \mu^-$ are [3]

$$\begin{aligned} \text{Br}(\bar{B} \rightarrow X_s \gamma) &= (3.49 \pm 0.19) \times 10^{-4}, \\ \text{Br}(B_s^0 \rightarrow \mu^+ \mu^-) &= (3.01 \pm 0.35) \times 10^{-9}. \end{aligned} \quad (32)$$

The newly introduced scalars in the FDM including CP-even Higgs, CP-odd Higgs and charged Higgs can make contributions to these two processes, the analytical calculations of the contributions are collected in the appendix [39].

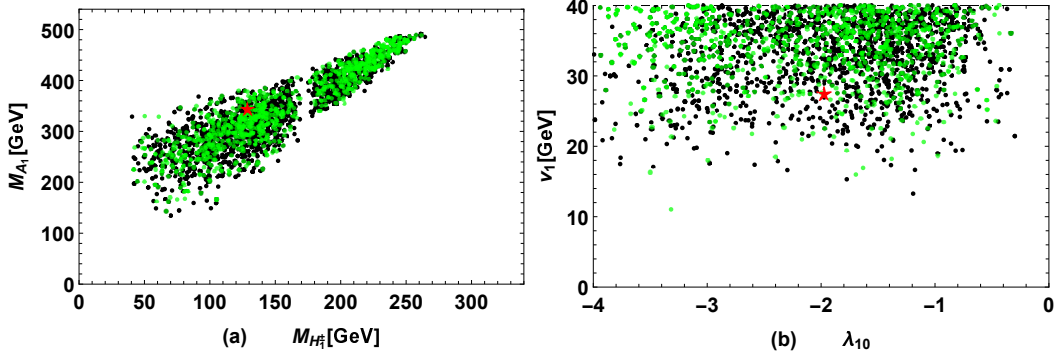


FIG. 5: Scanning the parameter spaces in Eq. (22), Eq. (31), Eq. (33) and keeping $0.2243 < |V_{us}| < 0.2263$, $0.003516 < |V_{ub}| < 0.003716$, $0.4139 < |V_{cb}| < 0.4159$, M_{H_2} in the range $124 \text{ GeV} < M_{H_2} < 126 \text{ GeV}$, the allowed ranges of $M_{H_{1^\pm}} - M_{A_1}$ (a) and $v_1 - \lambda_{10}$ (b) are plotted, where the black points, green points denote the results for $\text{Br}(\bar{B} \rightarrow X_s \gamma)$ and $\text{Br}(B_s^0 \rightarrow \mu^+ \mu^-)$ in the experimental 2σ , 1σ intervals respectively, the ‘red star’ denotes the best fit with the B meson rare decay branching ratios in Eq. (32) corresponding to $\chi^2 = \mathbf{0.022}$.

Scanning the parameter spaces in Eq. (22), Eq. (31) and the parameters $|m_{e,13}|$, $\theta_{e,ij}$, ($ij = 12, 13, 23$) in the following range

$$|m_{e,13}| = (0.0 \sim 0.3) \text{ GeV}, \theta_{e,ij} = (-\pi \sim \pi), \quad (33)$$

keeping $0.2243 < |V_{us}| < 0.2263$, $0.003516 < |V_{ub}| < 0.003716$, $0.4139 < |V_{cb}| < 0.4159$ and M_{H_2} in the range $124 \text{ GeV} < M_{H_2} < 126 \text{ GeV}$, we plot $M_{H_{1^\pm}} - M_{A_1}$, $v_1 - \lambda_{10}$ in Fig. 5 (a), Fig. 5 (b) respectively, where the black points, green points denote the results for $\text{Br}(\bar{B} \rightarrow X_s \gamma)$ and $\text{Br}(B_s^0 \rightarrow \mu^+ \mu^-)$ in the experimental 2σ , 1σ intervals respectively, the ‘red star’ denotes the best fit with the B meson rare decay branching ratios in Eq. (32) corresponding to $\chi^2 = 0.022$. The results of this best fit are listed in Tab. III.

For the parameters not shown in Fig. 5 such as $\lambda_1, \lambda_2, \dots$, they affect the predicted $\text{Br}(\bar{B} \rightarrow X_s \gamma)$ and $\text{Br}(B_s^0 \rightarrow \mu^+ \mu^-)$ mildly. The results presented in Fig. 5 (a) indicate that $M_{H_{1^\pm}}$ is correlated strongly to M_{A_1} because both of them mainly depend on λ_{10} as shown in Fig. 3 (a) and Fig. 4 (a). Eq. (13) and Eq. (14) show that the Yukawa couplings increase with decreasing v_1 , i.e. the scalars in the FDM can make significant contributions

Observables	O_i^{th}	O_i^{exp}	Deviations in %
$m_u[\text{MeV}]$	2.154	2.16	0.28
$m_c[\text{GeV}]$	1.658	1.67	0.72
$m_t[\text{GeV}]$	172.5	172.5	0
$m_d[\text{MeV}]$	4.67	4.67	0
$m_s[\text{MeV}]$	93.4	93.4	0
$m_b[\text{GeV}]$	4.78	4.78	0
$ v_{us} $	0.2252	0.2253	0.044
$ v_{ub} $	0.003617	0.003616	0.028
$ v_{cb} $	0.4138	0.04149	0
$\text{Br}(\bar{B} \rightarrow X_s \gamma)$	3.49×10^{-4}	3.49×10^{-4}	0
$\text{Br}(B_s^0 \rightarrow \mu^+ \mu^-)$	3.03×10^{-9}	3.01×10^{-9}	0.66

TABLE III: Fit with the B meson rare decays: the results obtained for the best fit corresponding to $\chi^2 = \mathbf{0.022}$.

to the B meson rare decay processes $\bar{B} \rightarrow X_s \gamma$, $B_s^0 \rightarrow \mu^+ \mu^-$ for small v_1 , which leads to the experimental observations of $\text{Br}(\bar{B} \rightarrow X_s \gamma)$ and $\text{Br}(B_s^0 \rightarrow \mu^+ \mu^-)$ prefer large v_1 , and Fig. 5 (b) shows that v_1 is limited in the range $v_1 \gtrsim 15$ GeV.

B. top quark rare decay processes $t \rightarrow ch$ and $t \rightarrow uh$

The branching ratios of the top quark rare decay processes $t \rightarrow ch$ and $t \rightarrow uh$ can be written as [40]

$$\text{Br}(t \rightarrow q_u h) = \frac{|\mathcal{M}_{tq_u h}|^2 \sqrt{((m_t + m_h)^2 - m_{q_u}^2)((m_t - m_h)^2 - m_{q_u}^2)}}{32\pi m_t^3 \Gamma_{\text{total}}^t}, \quad (34)$$

where $q_u = u, c$, the amplitude $\mathcal{M}_{tq_u h}$ can be read directly from the Yukawa couplings in Eq. (11), and $\Gamma_{\text{total}}^t = 1.42$ GeV [3] is the total decay width of top quark. The measured quark masses, CKM matrix and B meson rare decay processes $\bar{B} \rightarrow X_s \gamma$, $B_s^0 \rightarrow \mu^+ \mu^-$ should be considered in the calculations of top quark rare decay processes $t \rightarrow ch$ and $t \rightarrow uh$, hence we take the points obtained in Fig. 5 as inputs.

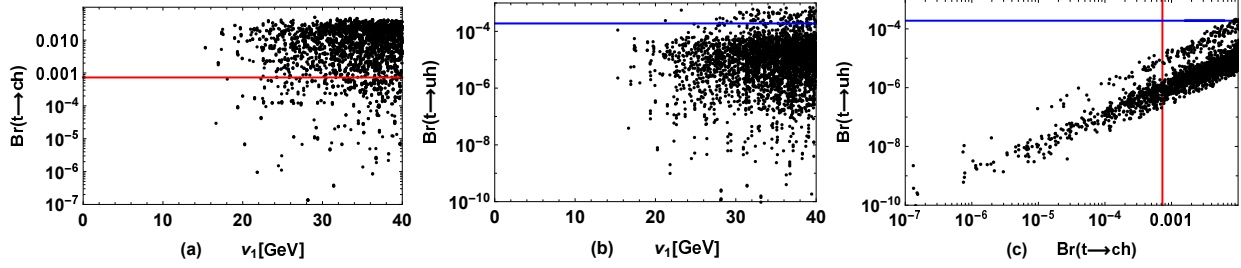


FIG. 6: Taking the points obtained in Fig. 5 as inputs, the results of $\text{Br}(t \rightarrow ch)$ versus $|m_{u,13}|$ (a), $\theta_{u,12}$ (b) and the results of $\text{Br}(t \rightarrow uh)$ versus $|m_{u,13}|$ (c), $\theta_{u,12}$ (d) are plotted, where red and blue lines denote the upper bounds on $\text{Br}(t \rightarrow ch)$ and $\text{Br}(t \rightarrow uh)$ from Particle Data Group [3] respectively.

Then we plot the results of $\text{Br}(t \rightarrow ch)$ versus v_1 in Fig. 6 (a), $\text{Br}(t \rightarrow uh)$ versus v_1 in Fig. 6 (b), and $\text{Br}(t \rightarrow ch)$ versus $\text{Br}(t \rightarrow uh)$ in Fig. 6 (c). The red and blue lines in Fig. 6 denote the upper bounds on $\text{Br}(t \rightarrow ch)$ and $\text{Br}(t \rightarrow uh)$ from Particle Data Group [3] respectively. The picture illustrates that the results of $\text{Br}(t \rightarrow ch)$, $\text{Br}(t \rightarrow uh)$ obtained in the FDM can be large, which indicates that the processes $t \rightarrow ch$, $t \rightarrow uh$ have great opportunities to be observed experimentally. In addition, the parameter space of the model suffers constraints from the experimental upper bounds on $\text{Br}(t \rightarrow ch)$ and $\text{Br}(t \rightarrow uh)$.

C. Lepton flavor violation processes $\tau \rightarrow 3e$, $\tau \rightarrow 3\mu$ and $\mu \rightarrow 3e$

Finally, we focus on the lepton flavor violation processes $\tau \rightarrow 3e$, $\tau \rightarrow 3\mu$, $\mu \rightarrow 3e$ predicted in the FDM. The corresponding amplitude can be written as [41]

$$\begin{aligned}
\mathcal{M}(e_j \rightarrow e_i e_i \bar{e}_i) = & C_1^L \bar{u}_{e_i}(p_2) \gamma_\mu P_L u_{e_j}(p_1) u_{e_i}(p_3) \gamma^\mu P_L \nu_{e_i}(p_4) \\
& + C_1^R \bar{u}_{e_i}(p_2) \gamma_\mu P_R u_{e_j}(p_1) u_{e_i}(p_3) \gamma^\mu P_R \nu_{e_i}(p_4) \\
& + [C_2^L \bar{u}_{e_i}(p_2) \gamma_\mu P_L u_{e_j}(p_1) u_{e_i}(p_3) \gamma^\mu P_R \nu_{e_i}(p_4) \\
& + C_2^R \bar{u}_{e_i}(p_2) \gamma_\mu P_R u_{e_j}(p_1) u_{e_i}(p_3) \gamma^\mu P_L \nu_{e_i}(p_4) - (p_2 \leftrightarrow p_3)] \\
& + [C_3^L \bar{u}_{e_i}(p_2) P_L u_{e_j}(p_1) u_{e_i}(p_3) P_L \nu_{e_i}(p_4) \\
& + C_3^R \bar{u}_{e_i}(p_2) P_R u_{e_j}(p_1) u_{e_i}(p_3) P_R \nu_{e_i}(p_4) - (p_2 \leftrightarrow p_3)], \tag{35}
\end{aligned}$$

Branching ratios	Present limit	Future sensitivity
$\text{Br}(\tau \rightarrow 3e)$	$< 2.7 \times 10^{-8}$	$\sim 10^{-10}$
$\text{Br}(\tau \rightarrow 3\mu)$	$< 2.1 \times 10^{-8}$	$\sim 10^{-10}$
$\text{Br}(\mu \rightarrow 3e)$	$< 10^{-12}$	$\sim 10^{-16}$

TABLE IV: Present limits and future sensitivities for the branching ratios for the LFV processes $\tau \rightarrow 3e$, $\tau \rightarrow 3\mu$ and $\mu \rightarrow 3e$ [3, 42, 43].

where $i = 1, 2$ for $j = 3$, $i = 1$ for $j = 2$, u_{e_i} denotes the spinor of lepton, ν_{e_i} denotes the spinor of antilepton, $P_L = (1 - \gamma_5)/2$, $P_R = (1 + \gamma_5)/2$, and p_k denotes the momentum of charged lepton with $k = 1, 2, 3, 4$. The coefficients $C_{1,2,3}^{L,R}$ from the contributions of Higgs bosons and Z, Z' gauge bosons, can be obtained through the Yukawa couplings in Eq. (11) and the definition of covariant derivative in Eq. (17). Then we can calculate the decay rate [41]

$$\Gamma(e_j \rightarrow e_i e_i \bar{e}_i) = \frac{m_{e_j}^5}{1536\pi^3} \left[\frac{1}{2} (|C_1^L|^2 + |C_1^R|^2) + |C_2^L|^2 + |C_2^R|^2 + \frac{1}{8} (|C_3^L|^2 + |C_3^R|^2) \right]. \quad (36)$$

The total decay widths of μ, τ are taken as $\Gamma_{\text{total}}^\mu = 2.996 \times 10^{-19}$ GeV, $\Gamma_{\text{total}}^\tau = 2.265 \times 10^{-12}$ GeV [3].

Scanning the free parameter space in Eq. (31), Eq. (33) and

$$g_F = (0, 0.8), \quad g_F = (-0.8, 0.8), \quad (37)$$

we plot the results of $\text{Br}(\tau \rightarrow 3e)$ versus $|m_{e,13}|$, $\text{Br}(\tau \rightarrow 3\mu)$ versus $\theta_{e,23}$, $\text{Br}(\mu \rightarrow 3e)$ versus $\theta_{e,12}$ in Fig. 7 (a), (b), (c) respectively by keeping M_{H_2} in the range $124 \text{ GeV} < M_{H_2} < 126 \text{ GeV}$ and $\text{Br}(\tau \rightarrow 3e) < 10^{-7}$, $\text{Br}(\tau \rightarrow 3\mu) < 10^{-7}$, $\text{Br}(\mu \rightarrow 3e) < 2 \times 10^{-12}$, then the allowed ranges of $v_\chi - v_1$, $g_F - g_{YF}$, $M_{Z'} - g_F$ are plotted in Fig. 7 (d), (e), (f) respectively. The gray points in Fig. 7 are excluded by the present limits, and the green points denote the results which can reach future experimental sensitivities, where the present limits and future sensitivities for the branching ratios of these LFV processes are listed in Tab. IV.

Fig. 7 (a), (b), (c) show that the experimental upper bounds on $\text{Br}(\tau \rightarrow 3\mu)$, $\text{Br}(\mu \rightarrow 3e)$ limit the parameter space strictly while the predicted $\text{Br}(\tau \rightarrow 3e)$ is less than about 10^{-12} which is hard to be observed in near future. In addition, the model predicts $\text{Br}(\tau \rightarrow$

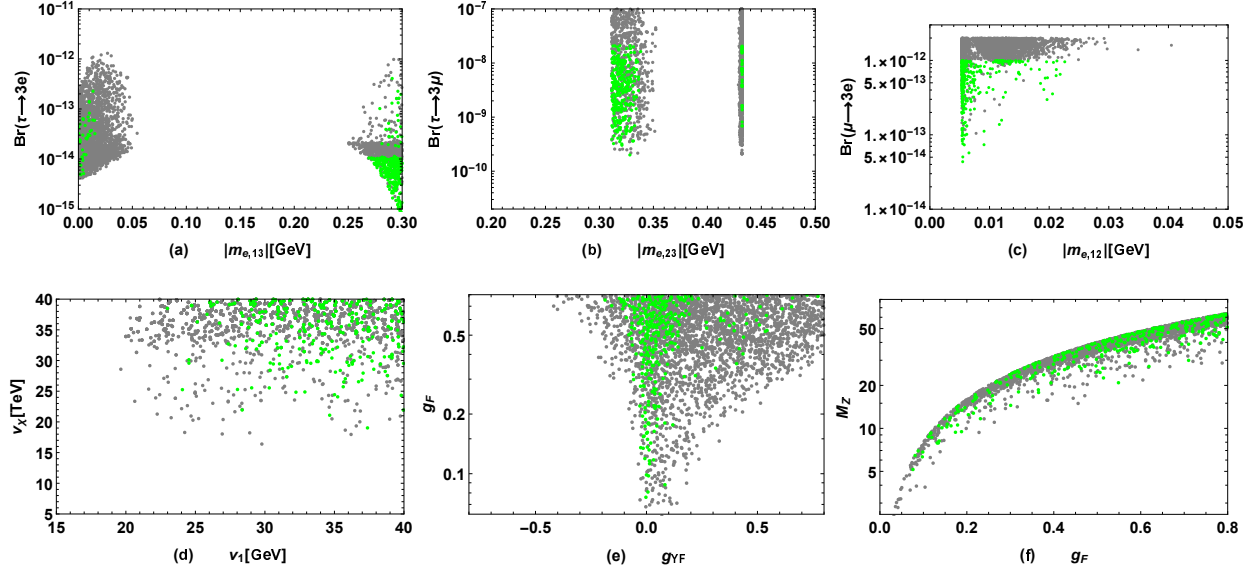


FIG. 7: Scanning the parameter space Eq. (31), Eq. (33), Eq. (37) and keeping M_{H_2} in the range $124 \text{ GeV} < M_{H_2} < 126 \text{ GeV}$ and $\text{Br}(\tau \rightarrow 3e) < 10^{-7}$, $\text{Br}(\tau \rightarrow 3\mu) < 10^{-7}$, $\text{Br}(\mu \rightarrow 3e) < 2 \times 10^{-12}$, the results of $\text{Br}(\tau \rightarrow 3e)$ versus $|m_{e,13}|$ (a), $\text{Br}(\tau \rightarrow 3\mu)$ versus $\theta_{e,23}$ (b), $\text{Br}(\mu \rightarrow 3e)$ versus $\theta_{e,12}$ (c) and the allowed ranges of $v_\chi - v_1$ (d), $g_F - g_{YF}$ (e), $M_{Z'} - g_F$ (f) are plotted, where the gray points are excluded by the present limits, the green points denote the results which can reach future experimental sensitivities.

$3\mu) \gtrsim 2 \times 10^{-10}$, $\text{Br}(\mu \rightarrow 3e) \gtrsim 5 \times 10^{-14}$, which indicates observing the LFV processes $\tau \rightarrow 3\mu$ and $\mu \rightarrow 3e$ is also effective to test the FDM. It is obvious in Fig. 7 (d) that the experimental upper bounds on the branching ratios of these LFV processes limit $v_1 \gtrsim 23 \text{ GeV}$, $v_\chi \gtrsim 20 \text{ TeV}$. Fig. 7 (e) indicates experimental constraints prefer $-0.2 \lesssim g_{YF} \lesssim 0.2$ and $g_{YF} \lesssim -0.2$ is excluded completely. From Fig. 7 (f), it can be seen explicitly that the allowed range of $M_{Z'}$ is related closely with the chosen value of g_F and $M_{Z'} \gtrsim 5 \text{ TeV}$.

V. SUMMARY

Motivated by the hierarchical structure of fermionic masses puzzle and fermionic flavor mixings puzzle, we propose a flavor-dependent model (FDM) to relate these two puzzles,

i.e. the proposed FDM can explain the flavor mixings puzzle and mass hierarchy puzzle simultaneously. The model extends the SM by an extra $U(1)_F$ local gauge group, two scalar doublets, one scalar singlet and two right-handed neutrinos, where the new $U(1)_F$ charges are related to the particles' flavor. In the FDM, only the third generation of quarks and charged leptons achieve the masses at the tree level, the first two generations achieve masses through the mixings with the third generation, and the neutrinos obtain tiny Majorana masses through the so-called Type I see-saw mechanism. In addition, the B meson rare decay processes $\bar{B} \rightarrow X_s \gamma$, $B_s^0 \rightarrow \mu^+ \mu^-$, the top quark rare decay processes $t \rightarrow ch$, $t \rightarrow uh$ and the τ LFV processes $\tau \rightarrow 3e$, $\tau \rightarrow 3\mu$, $\mu \rightarrow 3e$ predicted in the FDM are analyzed. It is found that observing the top quark rare decay processes $t \rightarrow ch$, $t \rightarrow uh$ and the τ LFV decays $\tau \rightarrow 3\mu$, $\mu \rightarrow 3e$ is effective to test the FDM, while τ LFV decay $\tau \rightarrow 3e$ is hard to be observed experimentally. In addition, the model can fit the observed quark masses, CKM matrix, $\text{Br}(\bar{B} \rightarrow X_s \gamma)$, $\text{Br}(B_s^0 \rightarrow \mu^+ \mu^-)$ well, and the VEVs of the two extra scalar doublets are limited to be larger than about 23 GeV, new Z' gauge boson is heavier than about 5 TeV and gauge kinetic mixing constant g_{YF} is larger than -0.2 by considering the experimental upper bounds on the branching ratios of LFV decays $\tau \rightarrow 3\mu$, $\mu \rightarrow 3e$.

Appendix A: Contributions to $\bar{B} \rightarrow X_s \gamma$ and $B_s^0 \rightarrow \mu^+ \mu^-$ in the FDM.

Generally, the effective Hamilton for the transition $b \rightarrow s$ at hadronic scale can be written as

$$H_{eff} = -\frac{4G_F}{\sqrt{2}} V_{ts}^* V_{tb} \left[C_1 \mathcal{O}_1^c + C_2 \mathcal{O}_2^c + \sum_{i=3}^6 \mathcal{O}_i + \sum_{i=7}^{10} (C_i \mathcal{O}_i + C'_i \mathcal{O}'_i) + \sum_{i=S,P} (C_i \mathcal{O}_i + C'_i \mathcal{O}'_i) \right], \quad (\text{A1})$$

where [44–49]

$$\begin{aligned} \mathcal{O}_1^u &= (\bar{s}_L \gamma_\mu T^a u_L) (\bar{u}_L \gamma^\mu T^a b_L), & \mathcal{O}_2^u &= (\bar{s}_L \gamma_\mu u_L) (\bar{u}_L \gamma^\mu b_L), \\ \mathcal{O}_3 &= (\bar{s}_L \gamma_\mu b_L) \sum_q (\bar{q} \gamma^\mu q), & \mathcal{O}_4 &= (\bar{s}_L \gamma_\mu T^a b_L) \sum_q (\bar{q} \gamma^\mu T^a q), \\ \mathcal{O}_5 &= (\bar{s}_L \gamma_\mu \gamma_\nu \gamma_\rho b_L) \sum_q (\bar{q} \gamma^\mu \gamma^\nu \gamma^\rho q), & \mathcal{O}_6 &= (\bar{s}_L \gamma_\mu \gamma_\nu \gamma_\rho T^a b_L) \sum_q (\bar{q} \gamma^\mu \gamma^\nu \gamma^\rho T^a q), \end{aligned}$$

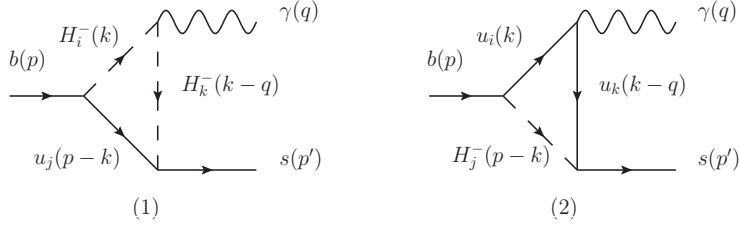


FIG. 8: The one loop Feynman diagrams contributing to $\bar{B} \rightarrow X_s \gamma$ from charged Higgs in the FDM.

$$\begin{aligned}
\mathcal{O}_7 &= \frac{e}{16\pi^2} m_b (\bar{s}_L \sigma_{\mu\nu} b_R) F^{\mu\nu}, & \mathcal{O}'_7 &= \frac{e}{16\pi^2} m_b (\bar{s}_R \sigma_{\mu\nu} b_L) F^{\mu\nu}, \\
\mathcal{O}_8 &= \frac{g_s}{16\pi^2} m_b (\bar{s}_L \sigma_{\mu\nu} T^a b_R) G^{a,\mu\nu}, & \mathcal{O}'_8 &= \frac{g_s}{16\pi^2} m_b (\bar{s}_R \sigma_{\mu\nu} T^a b_L) G^{a,\mu\nu}, \\
\mathcal{O}_9 &= \frac{e^2}{g_s^2} (\bar{s}_L \gamma_\mu b_L) \bar{l} \gamma^\mu l, & \mathcal{O}'_9 &= \frac{e^2}{g_s^2} (\bar{s}_R \gamma_\mu b_R) \bar{l} \gamma^\mu l, \\
\mathcal{O}_{10} &= \frac{e^2}{g_s^2} (\bar{s}_L \gamma_\mu b_L) \bar{l} \gamma^\mu \gamma_5 l, & \mathcal{O}'_{10} &= \frac{e^2}{g_s^2} (\bar{s}_R \gamma_\mu b_R) \bar{l} \gamma^\mu \gamma_5 l, \\
\mathcal{O}_S &= \frac{e^2}{16\pi^2} m_b (\bar{s}_L b_R) \bar{l} l, & \mathcal{O}'_S &= \frac{e^2}{16\pi^2} m_b (\bar{s}_R b_L) \bar{l} l, \\
\mathcal{O}_P &= \frac{e^2}{16\pi^2} m_b (\bar{s}_L b_R) \bar{l} \gamma_5 l, & \mathcal{O}'_P &= \frac{e^2}{16\pi^2} m_b (\bar{s}_R b_L) \bar{l} \gamma_5 l.
\end{aligned} \tag{A2}$$

In the definitions above, g_s is the strong coupling constant, T^a ($a = 1, \dots, 8$) are $SU(3)$ generators, $F^{\mu\nu}$ and $G^{\mu\nu}$ are the electromagnetic and gluon field strength tensors respectively.

The dominant contributions to $b \rightarrow s \gamma$ come from the charged Higgs in the FDM, and the leading-order Feynman diagrams are plotted in Fig. 8. Then the branching ratio of $\bar{B} \rightarrow X_s \gamma$ can be written as

$$Br(\bar{B} \rightarrow X_s \gamma) = R \left(|C_{7\gamma}(\mu_b)|^2 + N(E_\gamma) \right), \tag{A3}$$

where the overall factor $R = 2.47 \times 10^{-3}$, and the nonperturbative contribution $N(E_\gamma) = (3.6 \pm 0.6) \times 10^{-3}$ [50]. $C_{7\gamma}(\mu_b)$ can be written as

$$C_{7\gamma}(\mu_b) = C_{7\gamma,SM}(\mu_b) + C_{7\gamma,NP}(\mu_b), \tag{A4}$$

where the hadron scale $\mu_b = 2.5$ GeV and $C_{7\gamma,SM}(\mu_b) = -0.3689$ for the SM contribution at NNLO level [50–53]. In new physics models, the corresponding Wilson coefficients at the

bottom quark scale are [54, 55]

$$C_{7,NP}(\mu_b) \approx 0.5696C_{7,NP}(\mu_{EW}) + 0.1107C_{8,NP}(\mu_{EW}), \quad (\text{A5})$$

where

$$\begin{aligned} C_{7,NP}^{NP}(\mu_{EW}) &= C_{7,NP}^{(1)}(\mu_{EW}) + C_{7,NP}^{(2)}(\mu_{EW}) + C_{7,NP}'^{(1)}(\mu_{EW}) + C_{7,NP}'^{(2)}(\mu_{EW}), \\ C_{8,NP}(\mu_{EW}) &= C_{8g,NP}(\mu_{EW}) + C_{8g,NP}'(\mu_{EW}), \end{aligned} \quad (\text{A6})$$

The coefficients $C_{7,NP}^{(1,2)}(\mu_{EW})$ are Wilson coefficients of the process $b \rightarrow s\gamma$ and can be calculated from the diagrams in Fig. 8 (1), (2) respectively, the results read

$$\begin{aligned} C_{7,NP}^{(1)}(\mu_{EW}) &= \sum_{H_i^-, u_j} \frac{s_W^2}{2e^2 V_{ts}^* V_{tb}} \left\{ \frac{1}{2} C_{H_i^- \bar{s} u_j}^R C_{H_i^- b \bar{u}_j}^L [-I_3(x_{u_j}, x_{H_i^-}) + I_4(x_{u_j}, x_{H_i^-})] + \right. \\ &\quad \left. \frac{m_{u_j}}{m_b} C_{H_i^- \bar{s} u_j}^L C_{H_i^- b \bar{u}_j}^L [-I_1(x_{u_j}, x_{H_i^-}) + I_3(x_{u_j}, x_{H_i^-})] \right\}, \\ C_{7,NP}^{(2)}(\mu_{EW}) &= \sum_{H_j^-, u_i} \frac{s_W^2}{3e^2 V_{ts}^* V_{tb}} \left\{ \frac{1}{2} C_{H_j^- \bar{s} u_i}^R C_{H_j^- b \bar{u}_i}^L [-I_1(x_{u_i}, x_{H_j^-}) + 2I_3(x_{u_i}, x_{H_j^-}) \right. \\ &\quad \left. - I_4(x_{u_i}, x_{H_j^-})] + \frac{m_{u_i}}{m_b} C_{H_j^- \bar{s} u_i}^L C_{H_j^- b \bar{u}_i}^L [I_1(x_{u_i}, x_{H_j^-}) - I_2(x_{u_i}, x_{H_j^-}) \right. \\ &\quad \left. - I_3(x_{u_i}, x_{H_j^-})] \right\}, \\ C_7'^{NP(a)}(\mu_{EW}) &= C_7'^{NP(a)}(\mu_{EW})(L \leftrightarrow R), (a = 1, 2), \end{aligned} \quad (\text{A7})$$

where $x_i = \frac{m_i^2}{m_W^2}$, $C_{abc}^{L,R}$ denotes the scalar parts of the interaction vertex about abc with a, b, c denoting the interactional particles, and the loop integral functions $I_{1,\dots,4}$ can be found in our previous work [39]. In addition, $C_{8g,NP}(\mu_{EW})$ and $C_{8g,NP}'(\mu_{EW})$ at electroweak scale are

$$\begin{aligned} C_{8g,NP}(\mu_{EW}) &= [C_{7,NP}^{(2)}(\mu_{EW}) + C_{7,NP}^{(3)}(\mu_{EW})]/Q_u, \\ C_{8g,NP}'(\mu_{EW}) &= C_{8g,NP}(\mu_{EW})(L \leftrightarrow R), \end{aligned} \quad (\text{A8})$$

where $Q_u = 2/3$.

The main Feynman diagrams contributing to $B_s^0 \rightarrow \mu^+ \mu^-$ are plotted in Fig. 9. At the electroweak energy scale μ_{EW} , the corresponding Wilson coefficients can be written as

$$C_{S,NP}(\mu_{EW}) = \frac{\sqrt{2} s_W c_W}{4m_b e^3 V_{ts}^* V_{tb}} \left[C_{S,NP}^{(1)}(\mu_{EW}) + C_{S,NP}^{(2)}(\mu_{EW}) + C_{S,NP}^{(3)}(\mu_{EW}) + C_{S,NP}^{(4)}(\mu_{EW}) \right]$$

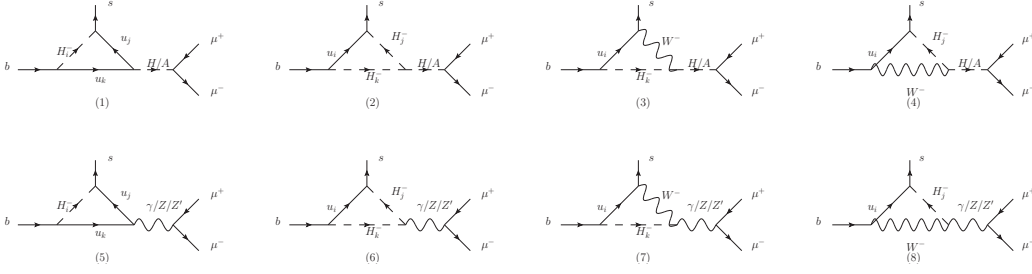


FIG. 9: The Feynman diagrams contributing to the decay $B_s^0 \rightarrow \mu^+ \mu^-$ in the B-LSSM

$$\begin{aligned}
& +C_{S,NP}^{(6)}(\mu_{EW})], \\
C'_{S,NP}(\mu_{EW}) &= C_{S,NP}(\mu_{EW})(L \leftrightarrow R), \\
C_{P,NP}(\mu_{EW}) &= \frac{\sqrt{2}s_W c_W}{4m_b e^3 V_{ts}^* V_{tb}} \left[C_{P,NP}^{(1)}(\mu_{EW}) + C_{P,NP}^{(2)}(\mu_{EW}) + C_{P,NP}^{(3)}(\mu_{EW}) + C_{P,NP}^{(4)}(\mu_{EW}) \right. \\
& \quad \left. + C_{P,NP}^{(6)}(\mu_{EW}) \right], \\
C'_{P,NP}(\mu_{EW}) &= -C_{P,NP}(\mu_{EW})(L \leftrightarrow R), \\
C_{9,NP}(\mu_{EW}) &= \frac{\sqrt{2}s_W c_W g_s^2}{64\pi^2 e^3 V_{ts}^* V_{tb}} \left[C_{9,NP}^{(5)}(\mu_{EW}) + C_{9,NP}^{(6)}(\mu_{EW}) + C_{9,NP}^{(7)}(\mu_{EW}) + C_{9,NP}^{(8)}(\mu_{EW}) \right], \\
C'_{9,NP}(\mu_{EW}) &= C_{9,NP}(\mu_{EW})(L \leftrightarrow R), \\
C_{10,NP}(\mu_{EW}) &= \frac{\sqrt{2}s_W c_W g_s^2}{64\pi^2 e^3 V_{ts}^* V_{tb}} \left[C_{10,NP}^{(5)}(\mu_{EW}) + C_{10,NP}^{(6)}(\mu_{EW}) + C_{10,NP}^{(7)}(\mu_{EW}) + C_{10,NP}^{(8)}(\mu_{EW}) \right], \\
C'_{10,NP}(\mu_{EW}) &= -C_{10,NP}(\mu_{EW})(L \leftrightarrow R). \tag{A9}
\end{aligned}$$

The superscripts (1, ..., 8) corresponding to the contributions in Fig. 9 (1,...,8) respectively and the results can be written as

$$\begin{aligned}
C_{S,NP}^{(1)}(\mu_{EW}) &= \sum_{H_i^-, u_j, u_k}^{S=H_1, A_1} \frac{C_{\bar{\mu}S\mu}^L + C_{\bar{\mu}S\mu}^R}{2(m_b^2 - m_S^2)} \left[C_{H_i^- \bar{s}u_j}^R C_{\bar{u}_j S u_k}^L C_{\bar{u}_k b H_i^-}^R G_2(x_{\tilde{H}_i^\pm}, x_{u_j}, x_{u_k}) \right. \\
& \quad \left. + m_{u_j} m_{u_k} C_{H_i^- \bar{s}u_j}^R C_{\bar{u}_j S u_k}^R C_{\bar{u}_k b H_i^-}^R G_1(x_{\tilde{H}_i^\pm}, x_{u_j}, x_{u_k}) \right], \\
C_{P,NP}^{(1)}(\mu_{EW}) &= \sum_{H_i^-, u_j, u_k}^{S=H_1, A_1} \frac{-C_{\bar{\mu}S\mu}^L + C_{\bar{\mu}S\mu}^R}{2(m_b^2 - m_S^2)} \left[C_{H_i^- \bar{s}u_j}^R C_{\bar{u}_j S u_k}^L C_{\bar{u}_k b H_i^-}^R G_2(x_{\tilde{H}_i^\pm}, x_{u_j}, x_{u_k}) \right. \\
& \quad \left. + m_{u_j} m_{u_k} C_{H_i^- \bar{s}u_j}^R C_{\bar{u}_j S u_k}^R C_{\bar{u}_k b H_i^-}^R G_1(x_{\tilde{H}_i^\pm}, x_{u_j}, x_{u_k}) \right], \tag{A10}
\end{aligned}$$

$$C_{S,NP}^{(2)}(\mu_{EW}) = \sum_{u_i, H_j^\pm, H_k^\pm}^{S=H_1, A_1} \frac{1}{2(m_b^2 - m_S^2)} m_{u_i} C_{\bar{s}u_i H_j^\pm}^R C_{\bar{u}_i b H_k^\pm}^R C_{S H_j^\pm H_k^\pm} G_1(x_{u_i}, x_{H_j^\pm}, x_{H_k^\pm})$$

$$\begin{aligned}
& \times (C_{\bar{\mu}S\mu}^L + C_{\bar{\mu}S\mu}^R), \\
C_{P,NP}^{(2)}(\mu_{EW}) &= \sum_{u_i, H_j^\pm, H_k^\pm}^{S=H_l, A_l} \frac{1}{2(m_b^2 - m_S^2)} m_{u_i} C_{\bar{s}u_i H_j^\pm}^R C_{\bar{u}_i b H_k^\pm}^R C_{SH_j^\pm H_k^\pm} G_1(x_{u_i}, x_{H_j^\pm}, x_{H_k^\pm}) \\
& \times (-C_{\bar{\mu}S\mu}^L + C_{\bar{\mu}S\mu}^R), \tag{A11}
\end{aligned}$$

$$\begin{aligned}
C_{S,NP}^{(3)}(\mu_{EW}) &= \sum_{u_i, H_k^\pm}^{S=H_l, A_l} \frac{-C_{W^\pm SH_k^\pm}}{2(m_b^2 - m_S^2)} \left[C_{\bar{s}W^\pm u_i}^L C_{\bar{u}_i H_k^\pm b}^R G_2(x_{u_i}, 1, x_{H_k^\pm}) - 2m_b m_{u_i} C_{\bar{s}W^\pm u_i}^L \right. \\
& \times \left. C_{\bar{u}_i H_k^\pm b}^L G_1(x_{u_i}, 1, x_{H_k^\pm}) \right] (C_{\bar{\mu}S\mu}^L + C_{\bar{\mu}S\mu}^R), \\
C_{P,NP}^{(3)}(\mu_{EW}) &= \sum_{u_i, H_k^\pm}^{S=H_l, A_l} \frac{-C_{W^\pm SH_k^\pm}}{2(m_b^2 - m_S^2)} \left[C_{\bar{s}W^\pm u_i}^L C_{\bar{u}_i H_k^\pm b}^R G_2(x_{u_i}, 1, x_{H_k^\pm}) - 2m_b m_{u_i} C_{\bar{s}W^\pm u_i}^L \right. \\
& \times \left. C_{\bar{u}_i H_k^\pm b}^L G_1(x_{u_i}, 1, x_{H_k^\pm}) \right] (-C_{\bar{\mu}S\mu}^L + C_{\bar{\mu}S\mu}^R), \tag{A12}
\end{aligned}$$

$$\begin{aligned}
C_{S,NP}^{(4)}(\mu_{EW}) &= \sum_{u_i, H_j^\pm}^{S=H_l, A_l} \frac{-C_{W^\pm SH_j^\pm}}{2(m_b^2 - m_S^2)} C_{\bar{s}H_j^\pm u_i}^R C_{\bar{u}_i W^\pm b}^R G_2(x_{u_i}, x_{H_j^\pm}, 1) (C_{\bar{\mu}S\mu}^L + C_{\bar{\mu}S\mu}^R), \\
C_{S,NP}^{(4)}(\mu_{EW}) &= \sum_{u_i, H_j^\pm}^{S=H_l, A_l} \frac{-C_{W^\pm SH_j^\pm}}{2(m_b^2 - m_S^2)} C_{\bar{s}H_j^\pm u_i}^R C_{\bar{u}_i W^\pm b}^R G_2(x_{u_i}, x_{H_j^\pm}, 1) (-C_{\bar{\mu}S\mu}^L + C_{\bar{\mu}S\mu}^R), \tag{A13}
\end{aligned}$$

$$\begin{aligned}
C_{9,NP}^{(5)}(\mu_{EW}) &= \sum_{\tilde{H}_i^\pm, u_j, u_k}^V \frac{C_{\bar{\mu}V\mu}^L + C_{\bar{\mu}V\mu}^R}{-2(m_b^2 - m_V^2)} \left[-\frac{1}{2} C_{H_i^\pm \bar{s}u_j}^R C_{\bar{u}_j V u_k}^R C_{u_k s H_i^\pm}^L G_2(x_{H_i^\pm}, x_{u_j}, x_{u_k}) \right. \\
& \left. + m_{u_j} m_{u_k} C_{H_i^\pm \bar{s}u_j}^R C_{\bar{u}_j V u_k}^L C_{\bar{u}_k s H_i^\pm}^L G_1(x_{H_i^\pm}, x_{u_j}, x_{u_k}) \right], \\
C_{10,NP}^{(5)}(\mu_{EW}) &= \sum_{\tilde{H}_i^\pm, u_j, u_k}^V \frac{-C_{\bar{\mu}V\mu}^L + C_{\bar{\mu}V\mu}^R}{-2(m_b^2 - m_V^2)} \left[-\frac{1}{2} C_{H_i^\pm \bar{s}u_j}^R C_{\bar{u}_j V u_k}^R C_{u_k s H_i^\pm}^L G_2(x_{H_i^\pm}, x_{u_j}, x_{u_k}) \right. \\
& \left. + m_{u_j} m_{u_k} C_{H_i^\pm \bar{s}u_j}^R C_{\bar{u}_j V u_k}^L C_{\bar{u}_k s H_i^\pm}^L G_1(x_{H_i^\pm}, x_{u_j}, x_{u_k}) \right], \tag{A14}
\end{aligned}$$

$$\begin{aligned}
C_{9,NP}^{(6)}(\mu_{EW}) &= \sum_{u_i, H_j^\pm, H_k^\pm}^V \frac{C_{\bar{\mu}V\mu}^L + C_{\bar{\mu}V\mu}^R}{4(m_b^2 - m_V^2)} C_{\bar{s}u_i H_j^\pm}^R C_{\bar{u}_i b H_k^\pm}^L C_{V H_j^\pm H_k^\pm} G_2(x_{u_i}, x_{H_j^\pm}, x_{H_k^\pm}), \\
C_{10,NP}^{(6)}(\mu_{EW}) &= \sum_{u_i, H_j^\pm, H_k^\pm}^V \frac{-C_{\bar{\mu}V\mu}^L + C_{\bar{\mu}V\mu}^R}{4(m_b^2 - m_V^2)} C_{\bar{s}u_i H_j^\pm}^R C_{\bar{u}_i b H_k^\pm}^L C_{V H_j^\pm H_k^\pm} G_2(x_{u_i}, x_{H_j^\pm}, x_{H_k^\pm}), \\
C_{S,NP}^{(6)}(\mu_{EW}) &= \sum_{u_i, H_j^\pm, H_k^\pm}^V \frac{C_{\bar{\mu}V\mu}^L + C_{\bar{\mu}V\mu}^R}{-2(m_b^2 - m_V^2)} m_b m_{u_i} C_{\bar{s}u_i H_j^\pm}^R C_{\bar{u}_i b H_k^\pm}^R C_{V H_j^\pm H_k^\pm} G_1(x_{u_i}, x_{H_j^\pm}, x_{H_k^\pm}),
\end{aligned}$$

$C_7^{eff,SM}$	$C_8^{eff,SM}$	$C_9^{eff,SM}$	$C_{10}^{eff,SM}$
-0.304	-0.167	4.211	-4.103

TABLE V: At hadronic scale $\mu = m_b$, SM Wilson coefficients to next-to-next-to-logarithmic accuracy.

$$C_{P,NP}^{(6)}(\mu_{EW}) = \sum_{u_i, H_j^\pm, H_k^\pm}^V \frac{C_{\bar{\mu}V\mu}^L - C_{\bar{\mu}V\mu}^R}{-2(m_b^2 - m_V^2)} m_b m_{u_i} C_{\bar{s}u_i H_j^\pm}^R C_{\bar{u}_i b H_k^\pm}^R C_{V H_j^\pm H_k^\pm} C_1(x_{u_i}, x_{H_j^\pm}, x_{H_k^\pm}), \quad (\text{A15})$$

$$C_{9,NP}^{(7)}(\mu_{EW}) = \sum_{u_i, H_k^\pm}^V \frac{C_{\bar{\mu}V\mu}^L + C_{\bar{\mu}V\mu}^R}{2(m_b^2 - m_V^2)} m_{u_i} C_{\bar{s}u_i W^\pm}^L C_{\bar{u}_i b H_k^\pm}^L C_{V W^\pm H_k^\pm} G_1(x_{u_i}, x_W, x_{H_k^\pm}),$$

$$C_{10,NP}^{(7)}(\mu_{EW}) = \sum_{u_i, H_k^\pm}^V \frac{-C_{\bar{\mu}V\mu}^L + C_{\bar{\mu}V\mu}^R}{2(m_b^2 - m_V^2)} m_{u_i} C_{\bar{s}u_i W^\pm}^L C_{\bar{u}_i b H_k^\pm}^L C_{V W^\pm H_k^\pm} G_1(x_{u_i}, x_W, x_{H_k^\pm}), \quad (\text{A16})$$

$$C_{9,NP}^{(8)}(\mu_{EW}) = \sum_{u_i, H_j^\pm}^V \frac{C_{\bar{\mu}V\mu}^L + C_{\bar{\mu}V\mu}^R}{2(m_b^2 - m_V^2)} m_{u_i} C_{\bar{s}u_i H_j^\pm}^R C_{\bar{u}_i b W^\pm}^L C_{V W^\pm H_k^\pm} G_1(x_{u_i}, x_{H_j^\pm}, x_W),$$

$$C_{10,NP}^{(8)}(\mu_{EW}) = \sum_{u_i, H_j^\pm}^V \frac{-C_{\bar{\mu}V\mu}^L + C_{\bar{\mu}V\mu}^R}{2(m_b^2 - m_V^2)} m_{u_i} C_{\bar{s}u_i H_j^\pm}^R C_{\bar{u}_i b W^\pm}^L C_{V W^\pm H_k^\pm} G_1(x_{u_i}, x_{H_j^\pm}, x_W), \quad (\text{A17})$$

where V denotes the vector bosons γ , Z , Z' , and C_{aVb} denote the scalar parts of the corresponding interaction vertex aVb . The concrete expressions for loop integral $G_k (k = 1, \dots, 4)$ can be found in the Appendix B of our previous work [39]. The Wilson coefficients at hadronic energy scale from the SM to next-to-next-to-logarithmic accuracy are shown in Table I. In addition, the Wilson coefficients in Eq. (A9) should be evolved down to hadronic scale $\mu \sim m_b$ by the renormalization group equations:

$$\vec{C}_{NP}(\mu) = \hat{U}(\mu, \mu_0) \vec{C}_{NP}(\mu_0),$$

$$\vec{C}_{NP}^{\hat{t}}(\mu) = \hat{U}^{\hat{t}}(\mu, \mu_0) \vec{C}_{NP}^{\hat{t}}(\mu_0) \quad (\text{A18})$$

with

$$\vec{C}_{NP}^T = (C_{1,NP}, \dots, C_{6,NP}, C_{7,NP}^{eff}, C_{8,NP}^{eff}, C_{9,NP}^{eff} - Y(q^2), C_{10,NP}^{eff}),$$

$$\vec{C}'_{NP,T} = (C'_{7,NP,eff}, C'_{8,NP,eff}, C'_{9,NP,eff}, C'_{10,NP,eff}). \quad (\text{A19})$$

Correspondingly, the evolving matrices $\widehat{U}(\mu, \mu_0)$, $\widehat{U}'(\mu, \mu_0)$ can be found in our previous work [39].

Then, the squared amplitude can be written as

$$|\mathcal{M}_s|^2 = 16G_F^2 |V_{tb}V_{ts}^*|^2 M_{B_s^0}^2 [|F_S^s|^2 + |F_P^s + 2m_\mu F_A^s|^2], \quad (\text{A20})$$

and

$$F_S^s = \frac{\alpha_{EW}(\mu_b)}{8\pi} \frac{m_b M_{B_s^0}^2}{m_b + m_s} f_{B_s^0} (C_S - C'_S), \quad (\text{A21})$$

$$F_P^s = \frac{\alpha_{EW}(\mu_b)}{8\pi} \frac{m_b M_{B_s^0}^2}{m_b + m_s} f_{B_s^0} (C_P - C'_P), \quad (\text{A22})$$

$$F_A^s = \frac{\alpha_{EW}(\mu_b)}{8\pi} f_{B_s^0} [C_{10}^{eff}(\mu_b) - C'_{10}{}^{eff}(\mu_b)], \quad (\text{A23})$$

where $f_{B_s^0} = (227 \pm 8)$ MeV denote the decay constants, $M_{B_s^0} = 5.367$ GeV denote the masses of neutral meson B_s^0 . The branching ratio of $B_s^0 \rightarrow \mu^+ \mu^-$ can be written as

$$Br(B_s^0 \rightarrow \mu^+ \mu^-) = \frac{\tau_{B_s^0}}{16\pi} \frac{|\mathcal{M}_s|^2}{M_{B_s^0}^2} \sqrt{1 - \frac{4m_\mu^2}{M_{B_s^0}^2}}, \quad (\text{A24})$$

with $\tau_{B_s^0} = 1.466(31)$ ps denoting the life time of meson.

Acknowledgments

The work has been supported by the National Natural Science Foundation of China (NNSFC) with Grants No. 12075074, No. 12235008, Hebei Natural Science Foundation with Grant No. A2022201017, No. A2023201041, Natural Science Foundation of Guangxi Autonomous Region with Grant No. 2022GXNSFDA035068, the youth top-notch talent support program of the Hebei Province.

[1] N. Cabibbo, Phys. Rev. Lett. **10**, 531-533 (1963).

[2] M. Kobayashi and T. Maskawa, Prog. Theor. Phys. **49**, 652-657 (1973).

- [3] R. L. Workman *et al.* [Particle Data Group], PTEP **2022**, 083C01 (2022).
- [4] C. D. Froggatt and H. B. Nielsen, Nucl. Phys. B **147**, 277-298 (1979).
- [5] Y. Koide, Phys. Lett. B **120**, 161-165 (1983).
- [6] M. Leurer, Y. Nir and N. Seiberg, Nucl. Phys. B **398**, 319-342 (1993).
- [7] L. E. Ibanez and G. G. Ross, Phys. Lett. B **332**, 100-110 (1994).
- [8] K. S. Babu and S. M. Barr, Phys. Lett. B **381**, 202-208 (1996).
- [9] Z. G. Berezhiani and M. Y. Khlopov, Sov. J. Nucl. Phys. **51**, 739-746 (1990)
- [10] Z. G. Berezhiani and M. Y. Khlopov, Sov. J. Nucl. Phys. **51**, 935-942 (1990)
- [11] A. S. Sakharov and M. Y. Khlopov, Phys. Atom. Nucl. **57**, 651-658 (1994)
- [12] L. Randall and R. Sundrum, Phys. Rev. Lett. **83**, 3370-3373 (1999).
- [13] D. E. Kaplan and T. M. P. Tait, JHEP **11**, 051 (2001).
- [14] M. C. Chen, D. R. T. Jones, A. Rajaraman and H. B. Yu, Phys. Rev. D **78**, 015019 (2008).
- [15] A. J. Buras, C. Grojean, S. Pokorski and R. Ziegler, JHEP **08**, 028 (2011).
- [16] S. F. King and C. Luhn, Rept. Prog. Phys. **76**, 056201 (2013).
- [17] S. F. King, A. Merle, S. Morisi, Y. Shimizu and M. Tanimoto, New J. Phys. **16**, 045018 (2014).
- [18] S. F. King, J. Phys. G **42**, 123001 (2015).
- [19] S. F. King, Prog. Part. Nucl. Phys. **94**, 217-256 (2017).
- [20] S. Weinberg, Phys. Rev. D **101**, no.3, 035020 (2020).
- [21] F. Feruglio and A. Romanino, Rev. Mod. Phys. **93**, no.1, 015007 (2021).
- [22] G. Abbas, Int. J. Mod. Phys. A **36**, no.18, 2150090 (2021).
- [23] G. Mohanta and K. M. Patel, Phys. Rev. D **106**, no.7, 075020 (2022).
- [24] G. Mohanta and K. M. Patel, JHEP **10**, 128 (2023).
- [25] G. Abbas, V. Singh, N. Singh and R. Sain, Eur. Phys. J. C **83**, no.4, 305 (2023).
- [26] S. Weinberg, Phys. Rev. Lett. **37**, 657 (1976).
- [27] L. Lavoura and H. Kuhbock, Eur. Phys. J. C **55**, 303-308 (2008).
- [28] I. P. Ivanov and E. Vdovin, Phys. Rev. D **86**, 095030 (2012).
- [29] R. González Felipe, H. Serôdio and J. P. Silva, Phys. Rev. D **87**, 055010 (2013).
- [30] R. Gonzalez Felipe, H. Serodio and J. P. Silva, Phys. Rev. D **88**, 015015 (2013).
- [31] V. Keus, S. F. King and S. Moretti, JHEP **01**, 052 (2014).

- [32] I. P. Ivanov and C. C. Nishi, JHEP **01**, 021 (2015).
- [33] N. Buskin and I. P. Ivanov, J. Phys. A **54**, 325401 (2021).
- [34] Y. Izawa, Y. Shimizu and H. Takei, PTEP **2023**, 063B04 (2023).
- [35] D. Van Loi and P. Van Dong, Eur. Phys. J. C **83**, no.11, 1048 (2023).
- [36] S. Weinberg, Phys. Rev. Lett. **43**, 1566-1570 (1979).
- [37] J. L. Yang, H. B. Zhang and T. F. Feng, Phys. Lett. B **853**, 138677 (2024).
- [38] B. W. Lee, C. Quigg and H. B. Thacker, Phys. Rev. D **16**, 1519 (1977)
- [39] J. L. Yang, T. F. Feng, S. M. Zhao, R. F. Zhu, X. Y. Yang and H. B. Zhang, Eur. Phys. J. C **78**, 714 (2018).
- [40] J. L. Yang, T. F. Feng, H. B. Zhang, G. Z. Ning and X. Y. Yang, Eur. Phys. J. C **78**, 438 (2018).
- [41] J. Hisano, T. Moroi, K. Tobe and M. Yamaguchi, Phys. Rev. D **53**, 2442-2459 (1996).
- [42] A. Blondel, A. Bravar, M. Pohl, S. Bachmann, N. Berger, M. Kiehn, A. Schoning, D. Wiedner, B. Windelband and P. Eckert, *et al.* [arXiv:1301.6113 [physics.ins-det]].
- [43] K. Hayasaka [Belle and Belle-II], J. Phys. Conf. Ser. **408**, 012069 (2013).
- [44] R. Grigjanis, P. J. O'Donnell, M. Sutherland and H. Navelet, Phys. Rep. **22**, 93 (1993).
- [45] G. Buchalla, A. J. Buras and M. E. Lautenbacher, Rev. Mod. Phys. **68**, 1125 (1996).
- [46] W. Altmannshofer, P. Ball, A. Bharucha, A. J. Buras, D. M. Straub and M. Wick, JHEP **0901**, 019 (2009) [arXiv:0811.1214 [hep-ph]].
- [47] L. Lin, T. F. Feng and F. Sun, Mod. Phys. Lett. A **24**, 2181-2186 (2009).
- [48] X. Y. Yang and T. F. Feng, JHEP **1005**, 059 (2010).
- [49] P. Goertz and T. Pfoh, Phys. Rev. D **84**, 095016 (2011).
- [50] A. J. Buras, L. Merlo, E. Stamou, JHEP **1108** 124 (2011).
- [51] F. Goertz, T. Pfoh, Phys. Rev. D **84** 095016 (2011).
- [52] P. Gambino, M. Misiak, Nucl. Phys. B **611** 338 (2001).
- [53] M. Czakon, U. Haisch, M. Misiak, JHEP **0703** 008 (2007).
- [54] A.J. Buras, M. Misiak, M. Müünz and S. Pokorski, Nucl. Phys. B **424** 374 (1994).
- [55] T. J. Gao, T. F. Feng, J. B. Chen, Mod. Phys. Lett. A **7** 1250011 (2012).